Author postprint version

A new elasmosaurid plesiosaurian from the Early Cretaceous of Russia marks an early attempt at neck elongation

Valentin Fischer[1]*, ,Nikolay G. Zverkov[2,3], ,Maxim S. Arkhangelsky[4,5], Ilya M. Stenshin[6], Ivan V. Blagovetshensky[7] And Gleb N. Uspensky[8]

[1] Evolution & Diversity Dynamics Lab, Université de Liège, 14 Allée du 6 Août, Liège 4000, Belgium
[2] Borissiak Paleontological Institute of the Russian Academy of Sciences, 123 Profsoyuznaya Street, Moscow 117647, Russia
[3] Geological Institute of the Russian Academy of Sciences, Pyzhevsky Lane 7, Moscow 119017, Russia
[4] Department of General Geology and Minerals, Saratov State University, A83 Astrakhanskaya Street, 410012 Saratov, Russia
[5] Department of Geoecology and Engineering Geology, Saratov State Technical University, 77 Politekhnicheskaya Street, 410054 Saratov, Russia
[6] Undory Paleontological Museum, Undory, Ulyanovsk Region 433312, Russia
[7] Department of Biology, Ecology and Nature Management, Ulyanovsk State University, Leo Tolstoy Street, Ulyanovsk 432000, Russia
[8] Natural Science Museum, Ulyanovsk State University, Leo Tolstoy Street, Ulyanovsk 432000, Russia Received 30 May 2020; revised 6 July 2020; accepted for publication 8 August 2020

Published: 16 October 2020 in *Zoological Journal of the Linnean Society*, zlaa103,
https://doi.org/10.1093/zoolinnean/zlaa103

Abstract

Plesiosaurian marine reptiles evolved a wide range of body shapes during the Jurassic and Cretaceous, including long-necked forms. Many Late Cretaceous members of the clade Elasmosauridae epitomized this part of the plesiosaurian morphological spectrum by evolving extremely long necks through somitogenesis (resulting in an increase in the number of cervical centra) and differential growth (resulting in the elongation of cervical centra). However, the early evolution of elasmosaurids remains poorly understood because of a generally poor Lower Cretaceous fossil record. We

describe a new elasmosaurid, *Jucha squalea* gen. et sp. nov., from the upper Hauterivian (Lower Cretaceous) of Ulyanovsk (European Russia), in addition to other elasmosaurid remains from the same area. *Jucha squalea* is one of the oldest and basalmost elasmosaurids known and lacks a series of features that otherwise characterize the group, such as the heart-shaped intercoracoid fenestra and the median pectoral bar. However, *Jucha squalea* marks an early attempt at cervical elongation through differential growth. The data we gathered on the shape of cervical centra among elasmosaurids suggest multiple episodes of elongation and shortening. However, the precise patterns are obscured by an unstable phylogenetic signal.

Cervical, elongation, differential growth, Hauterivian, marine reptiles, Xenopsaria

INTRODUCTION

Elasmosaurids are a clade of plesiosaurian marine reptiles notably characterized by an extreme elongation of the neck, which contains several dozens of centra, sometimes > 70 (O'Keefe, 2002; Kubo *et al.*, 2012; Sachs *et al.*, 2013; Soul & Benson, 2017). Elasmosaurids are part of a wider clade, Xenopsaria, that diversified markedly during the Cretaceous (Benson & Druckenmiller, 2014), evolving a range of distinct morphologies with varying relative neck lengths (O'Keefe, 2002; Benson & Druckenmiller, 2014; Otero, 2016; Serratos *et al.*, 2017; Fischer *et al.*, 2018). However, the early evolution of Xenopsaria and the initial diversification of its main clades, Elasmosauridae and Leptocleidia, are poorly known and in a state of flux, because only a few taxa are known from the Early Cretaceous and these frequently switch phylogenetic positions (e.g. compare Kear *et al.*, 2006; Benson *et al.*, 2013; Hampe, 2013; Benson & Druckenmiller, 2014; Sachs *et al.*, 2016; Serratos *et al.*, 2017; Fischer *et al.*, 2018; Páramo-Fonseca *et al.*, 2019b; O'Gorman, 2020).

Only a few elasmosaurid taxa are known from the entire Early Cretaceous: *Lagenanectes richterae* Sachs, Hornung & Kear, 2017 from the Hauterivian–Barremian of Germany, the yet unnamed Speeton plesiosaurians (NHMUK PV R8623 and SCARB 200751) from the Hauterivian of the UK (Benson & Druckenmiller, 2014), *Callawayasaurus colombiensis* (Welles, 1962) from the Aptian of Colombia, *Leivanectes bernardoi* Páramo-Fonseca *et al.*, 2019b from the Aptian of Colombia, *Wapuskanectes betsynichollsae* Druckenmiller & Russell, 2006 from the Albian of Canada and *Eromangasaurus australis* Kear, 2005 from the Albian of Australia (Sachs, 2005a; Kear, 2007). All the other putative elasmosaurid specimens from the Berriasian–Hauterivian interval are undetermined postcranial remains, from Western Europe (Fournier *et al.*,

1982), Russia (Dubeikovsky & Ochev, 1967; Berezin & Aleksandrov, 2016; Zverkov & Kiselev, 2018), Argentina (Lazo & Cichowolski, 2003; O'Gorman *et al.*, 2015a) and Colombia (Páramo-Fonseca, 2015). Moreover, *La. richterae* was recovered as a basal elasmosaurid in two analyses (Sachs *et al.*, 2017; Madzia & Cau, 2020) and as a basal leptocleidian or basal xenopsarian in two others (Sachs *et al.*, 2018; Páramo-Fonseca *et al.*, 2019b, respectively), further demonstrating the need for additional data to document the early history of elasmosaurids better.

We describe a new taxon and two other specimens from the upper Hauterivian of European Russia. This new taxon is recovered as one of the earliest elasmosaurids and lacks several features that otherwise characterize the group. We also analyse the patterns of cervical elongation through the evolutionary history of elasmosaurids. The new taxon marks an early case of cervical elongation, which re-evolves only by the Late Cretaceous.

MATERIAL AND METHODS

Institutional abbreviations

AMNH, American Museum of Natural History, New York, NY, USA; ANSP, Academy of Natural Sciences of Drexel University, Philadelphia, PA, USA; BGR, Bundesanstalt für Geowissenschaften und Rohstoffe, Hannover, Germany; GPMM, Geomuseum der Universität Münster, Westfalen, Germany; KUVP, Natural History Museum, University of Kansas, Lawrence, KS, USA; LACM, Natural History Museum of Los Angeles County, Los Angeles, CA, USA; MCS, Museo de Cinco Saltos, Río Negro Province, Argentina; MGUAN, Museu de Geologia da Universidade Agostinho Neto, Luanda, Angola; MLP, Museo de la Plata, Buenos Aires Province, Argentina; MOR, Museum of the Rockies, Bozeman, MT, USA; MOZ, Museo Juan Olsacher, Zapala, Neuquen Province, Argentina; NHMUK, Natural History Museum, London, UK; NZGS, New Zealand Geological Survey, Lower Hutt, New Zealand; RSM, Royal Saskatchewan Museum, Regina, Saskatchewan, Canada; SCARB, Rotunda Museum, Scarborough, UK; SGO, Museo Nacional de Historia Natural, Santiago, Chile; SMNK, Staatliches Museum für Naturkunde Karlsruhe, Germany; SMU SMP, Shuler Museum of Paleontology, Southern Methodist University, Dallas, TX, USA; SSU, Geological Museum, Saratov State University, Saratov, Russia; SU, Kagoshima Prefectural Museum, Shishijima, Japan; TMP, Royal Tyrrell

Museum of Paleontology, Drumheller, Alberta, Canada; UCMP, University of California Museum of Paleontology, Berkeley, CA, USA; UPM, Undory Palaeontological museum, Undory, Ulyanovsk Region, Russia; YKM, Ulyanovsk Regional Museum of Local Lore named after I. A. Goncharov, Ulyanovsk, Ulyanovsk Region, Russia; YSPU, Ushinsky State Pedagogical University, Yaroslavl, Russia.

Geography and stratigraphy

The right bank of the Volga River exposes Hauterivian to Barremian successions in the northern part of the Ulyanovsk district (European Russia). From the Slantsevy Rudnik village (formerly Zakharyevsky Rudnik) to the Polivno settlement (north of Ulyanovsk; Fig. 1), these successions are restricted to the upper Hauterivian–lower Barremian interval of the Klimovka Formation (Baraboshkin & Guzhikov, 2015). The Hauterivian deposits in the area have a thickness of ~50 m and consist of dark grey, poorly lithified shales, with occasional beds and lenses of siltite (Blagovetshenskiy & Shumilkin, 2006a). Several horizons contain large carbonate concretions ranging from 0.2 to 1.5 m in length; the shape of these concretions, colour of their matrix and the sequence of their diagenetic fracture filling can be used as stratigraphic markers, delineating several horizons across the succession. Despite a long history of bio- and lithostratigraphic studies initiated by Pavlow (1892), there is little consensus on the details of the biostratigraphic succession of the Lower Cretaceous successions along the Volga River, because a series of local schemes co-exists (Baraboshkin, 2004; Blagovetshenskiy & Shumilkin, 2006a, b; Baraboshkin & Blagoveschensky, 2010; Baraboshkin & Guzhikov, 2015, 2018). Based on our field observations (I.V.B. and I.M.S.) and layer-by-layer sampling of invertebrates (I.V.B.), we follow the divisions proposed by Pavlow (1892, 1901), who recognized two ammonite biozones in the upper Hauterivian of the region: the *Speetoniceras versicolor* Zone in the lower part of the Upper Hauterivian and the *Simbirskites decheni* Zone in the uppermost Hauterivian.

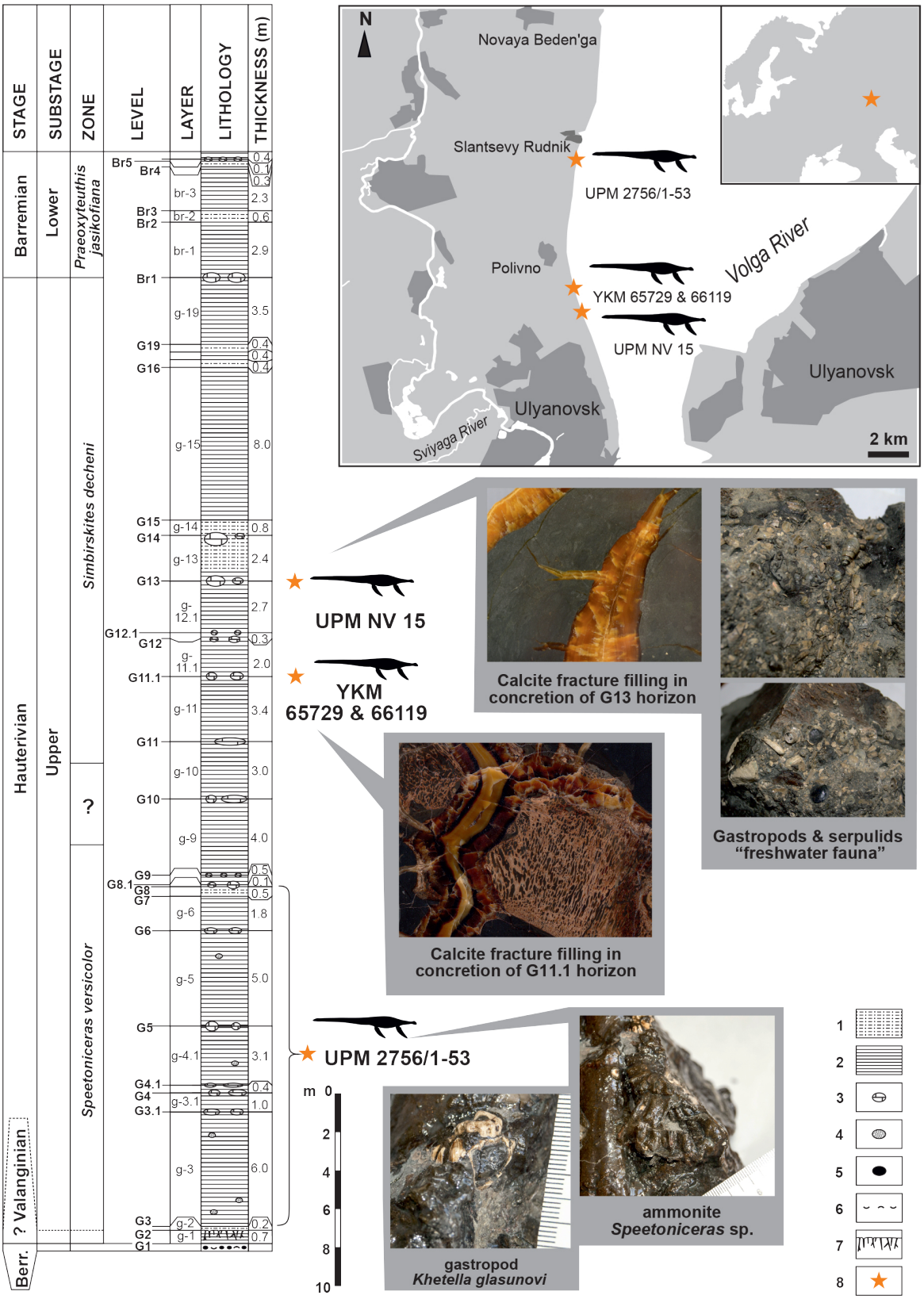

Figure 1. Spatiotemporal distribution of the specimens studied here and stratigraphic log of the relevant section of the Klimovka Formation, upper Hauterivian, Lower Cretaceous. Lithologies: 1, shale; 2, clay; 3, carbonate concretions; 4, pyrite concretions; 5, phosphorite nodules; 6, coquina bed; 7, bioturbated bed; 8, elasmosaurid remains.

The specimens UPM NV 15 and YKM 65729 + 66119 were collected near the Polivno settlement (Fig. 1), and the specimen UPM 2756/1-53 was collected near the Slantsevy Rudnik village. All these specimens originate from the Klimovka Formation, but their precise position within the formation is unclear because they were collected from landslides, at water level. However, the diagenesis of the bones, the structure of the enclosing concretions, and the associated invertebrate fauna can be used to refine their stratigraphic provenance.

The concretions enclosing some elements of the specimen UPM NV 15 contain the typical gastropod assemblage of the so-called 'freshwater fauna' of Kabanov (1959), even though the palaeoenvironment was clearly marine (Baraboshkin *et al.*, 2003). It includes gastropods *Crispotrochus humilis*(Trautschold, 1865), *Hudlestoniella pusilla* (Tullberg, 1881), *Tornatellaea kabanovi* Blagovetshenskiy, 2017 and multiple serpulids of the genus *Ditrupa*. This combination of taxa and, in places, the abundance of invertebrate fossils are unique to the local stratigraphic intervals G13–G15, corresponding to the lower half of the *Simbirskites decheni* Zone (Blagovetshenskiy & Shumilkin, 2006a). Within this interval, the sequence of light orange then white calcite fracture filling is typical of G13 horizon, enclosed within the *Simbirskites decheni* Zone (Fig. 1).

The specimen YKM 65729 + 66119 is preserved in two large clayey-carbonate concretions of irregular shape. Although no invertebrate remains are found with this specimen, the diagenetic filling sequence of the fractures in the concretion by dark then yellowish calcite is characteristic of G11.1 horizon, corresponding to the basal part of the *Simbirskites decheni* Zone.

The specimen UPM 2756/1-53 is covered by an external layer of pyrite that fills inner pores and that fused with the bone surface, which is typical of the vertebrate remains from the *Speetoniceras versicolor* Zone in the region (Fischer *et al.*, 2015, 2017; I. M. Stenshin, pers. obs.). A small ammonite, *Speetoniceras* sp., and a large specimen of the gastropod *Khetella Glazunov*Guzhov, 2004 are associated with the specimen (Fig. 1). *Khetella glasunovi* is abundant in the upper Hauterivian and present in both the *Speetoniceras versicolor* and the *Simbirskites decheni* zones. However, its specimens are commonly larger in size in the *Speetoniceras versicolor* Zone; the presence of an ammonite, *Speetoniceras* sp., associated with the specimen further supports this conclusion. This indicates that UPM 2756/1-53 belongs to the *Speetoniceras versicolor* Zone, like the holotype of the

pliosaurid *Makhaira rossica* Fischer *et al.*, 2015, which was found ~200 m north.

Phylogenetic analysis

We used the dataset of O'Gorman (2020), which is the most complete dataset for elasmosaurids to date. We updated the matrix by adding two putative elasmosaurid operational taxonomic units (OTUs): *La. richterae*, complementing the scores of Sachs *et al.* (2017) (which we obtained from B. Kear, pers. comm. April 2020) and the new species, *Jucha squalea*. Our scores for *J. squalea* are based solely on the holotype specimen. We also changed two scores of *Er. australis* based on first-hand examination of the holotype by one of us (V. Fischer): 155:0&1 and 165:1. We also added the polycotylid and pliosaurid data stemming from the work of Benson & Druckenmiller (2014) and updated by Fischer *et al.* (2015, 2017, 2018) and Serratos *et al.* (2017), in addition to data from the literature on non-elasmosaurids (Hampe, 1992; Gasparini & O'Gorman, 2014; Páramo-Fonseca *et al.*, 2016; Wintrich *et al.*, 2017; Madzia *et al.*, 2018; O'Gorman *et al.*, 2018; Páramo-Fonseca *et al.*, 2018, 2019a). O'Gorman (2020)added several elamosaurid-focused characters (13) but did not score for them most non-elasmosaurid OTUs; likewise, the data on polycotylids and pliosaurids we added is scored as '?' for these new characters, pending a thorough scoring of these new characters for non-elasmosaurids, which is not within the scope of this paper. The resulting dataset is a matrix of 131 taxa × 283 characters.

We then analysed this dataset in maximum parsimony using TNT v.1.5 (Goloboff & Catalano, 2016) with equal and implied weighting (with the default concavity constant, $k = 3$). In a maximum parsimony framework, implied weighting has been shown to yield clearly superior results, comparable to those of a Bayesian inference (Smith, 2019). In each case, we used the parsimony ratchet to carry out a rapid investigation of a series of shortest-tree islands (200 ratchet iterations and otherwise default options, with drift activated at ten iterations). The most parsimonious trees recovered by the parsimony ratchet where subjected to branch swapping using the tree bisection and reconnection (TBR) to maximize the recovery of most parsimonious trees; we set the maximal number of retained trees to 100 000. We provide our matrices containing the most parsimonious trees (one nexus file for the equal weighted analysis and one for the implied weighted analysis) and our TNT scripts as Supporting Information (supplementary files). We estimated the support for each clade using symmetric resampling, which is suitable for both unweighted and weighted parsimony analyses (Goloboff *et al.*, 2003). We used a 33% symmetric change probability and 10 000

replicates, using the clades of the first most parsimonious tree as the reference.

We computed the strict and the 50% majority rule consensus trees in R using the packages ape v.5.3 (Paradis *et al.*, 2004) and paleotree v.3.3 (Bapst, 2012). We time-scaled the consensus tree using the 'equal' method (Brusatte *et al.*, 2008), using the strap v.1.4 package (Bell & Lloyd, 2015) and a table describing the geological range (or age uncertainties) of each taxon in the phylogeny. This table (see Supporting Information, Table S1; supplementary files) was updated from a previous version (Fischer *et al.*, 2018) using the literature (Otero, 2016; Sachs *et al.*, 2017; O'Gorman, 2020).

Patterns of neck elongation

We gathered a series of measurements on the axial and appendicular skeletons of the three specimens described here (Tables 1 and 2). We assembled a dataset of anterior cervical centrum dimensions among elasmosaurids and basal leptocleidians. Although this approach does not use total neck lengths as in the study by Soul & Benson (2017), the taxonomic sampling is markedly increased, allowing incorporation of 29 elasmosaurids as opposed to between five and eight when complete necks are required. We obtained these data first hand (*Er. australis* and *J. squalea*) and from the literature (see Table 3). By convention, we focused our data on cervical centrum 10 (or the best-preserved centrum close to centrum 10), in order to investigate roughly similar regions of the anterior part of the neck. We gathered similar data on indeterminate Early Cretaceous elasmosaurids and on taxa not currently included in our phylogenetic dataset, such as '*Cimoliasaurus*' and *Styxosaurus browni* Welles, 1943, in order to obtain a more complete overview of the cervical elongation patterns in elasmosaurids. Given that the cervical centra with the greatest elongation are distributed inconsistently within elasmosaurid necks, we also assembled a second dataset, wherein we used the cervical centrum with the highest length-to-height ratio, regardless of its position within the neck (Table 3).

Table 1. Vertebral measurements (in millimetres) of *Jucha squalea* and cf. *Jucha*

Specimen	Region	Length	Medial height	Width
Jucha squalea, holotype (UPM 2756/1-53)	Cervical	38	30	34
Jucha squalea, holotype (UPM 2756/1-53)	Cervical	58	43	51

Specimen	Region	Length	Medial height	Width
Jucha squalea, holotype (UPM 2756/1-53)	Cervical	64	49	59
Jucha squalea, holotype (UPM 2756/1-53)	Cervical	70.5	52	67
Jucha squalea, holotype (UPM 2756/1-53)	Cervical	69	56	66
Jucha squalea, holotype (UPM 2756/1-53)	Cervical	70	56	69
Jucha squalea, holotype (UPM 2756/1-53)	Cervical	73	56	69
Jucha squalea, holotype (UPM 2756/1-53)	Cervical	78	61	76
Jucha squalea, holotype (UPM 2756/1-53)	Cervical	80	65	80
Jucha squalea, holotype (UPM 2756/1-53)	Cervical	79	68	81
Jucha squalea, holotype (UPM 2756/1-53)	Cervical	79	65	80
Jucha squalea, holotype (UPM 2756/1-53)	Cervical	82	70	82
Jucha squalea, holotype (UPM 2756/1-53)	Cervical	84	70	85
Jucha squalea, holotype (UPM 2756/1-53)	Cervical	84	72	87
Jucha squalea, holotype (UPM 2756/1-53)	Cervical*	79	71	87
Jucha squalea, holotype (UPM 2756/1-53)	Cervical*	83	NA	93
Jucha squalea, holotype (UPM 2756/1-53)	Cervical*	83	78	99
Jucha squalea, holotype (UPM 2756/1-53)	Cervical*	87	NA	102
Jucha squalea, holotype (UPM 2756/1-53)	Cervical	79	NA	100
Jucha squalea, holotype (UPM 2756/1-53)	Cervical	87	89	108
Jucha squalea, holotype (UPM 2756/1-53)	Cervical	85	89	108
Jucha squalea, holotype (UPM 2756/1-53)	Cervical	80	79	95

Specimen	Region	Length	Medial height	Width
Jucha squalea, holotype (UPM 2756/1-53)	Pectoral*	75	NA	100
Jucha squalea, holotype (UPM 2756/1-53)	Pectoral*	73	NA	100
Jucha squalea, holotype (UPM 2756/1-53)	Dorsal	70	NA	100
Jucha squalea, holotype (UPM 2756/1-53)	Dorsal*	74	NA	108
Jucha squalea, holotype (UPM 2756/1-53)	Dorsal*	72	NA	115
Jucha squalea, holotype (UPM 2756/1-53)	Dorsal*	~35	NA	120
Jucha squalea, holotype (UPM 2756/1-53)	Posterior dorsal*	74	83	100
Jucha squalea, holotype (UPM 2756/1-53)	Posterior dorsal*	73	NA	89
Jucha squalea, holotype (UPM 2756/1-53)	Posterior dorsal*	70	NA	90
Jucha squalea, holotype (UPM 2756/1-53)	Posterior dorsal*	74	NA	99
Jucha squalea, holotype (UPM 2756/1-53)	Posterior dorsal*	72	NA	95
Jucha squalea, holotype (UPM 2756/1-53)	Posterior dorsal*	72	NA	99
Jucha squalea, holotype (UPM 2756/1-53)	Posterior dorsal*	65	NA	95
Jucha squalea, holotype (UPM 2756/1-53)	Posterior dorsal*	62	NA	89
Jucha squalea, holotype (UPM 2756/1-53)	Posterior dorsal*	59	NA	86
Jucha squalea, holotype (UPM 2756/1-53)	Posterior dorsal*	58	NA	91
Jucha squalea, holotype (UPM 2756/1-53)	Posterior dorsal*	61	72	89
Jucha squalea, holotype (UPM 2756/1-53)	Posterior dorsal*	58	69	79
Jucha squalea, holotype (UPM 2756/1-53)	Posterior dorsal	75	NA	81
Jucha squalea, holotype (UPM 2756/1-53)	Sacral	56	65	78

Specimen	Region	Length	Medial height	Width
Jucha squalea, holotype (UPM 2756/1-53)	Caudal*	45	61	69
Jucha squalea, holotype (UPM 2756/1-53)	Caudal*	45	NA	NA
Jucha squalea, holotype (UPM 2756/1-53)	Caudal*	42	NA	79
cf. *Jucha* (UPM NV 15)	Cervical	57.4	42.8	51.3
cf. *Jucha* (UPM NV 15)	Cervical	63	45.9	56.8
cf. *Jucha* (UPM NV 15)	Cervical	65.1	47	57.7
cf. *Jucha* (UPM NV 15)	Cervical	68.6	49	62
cf. *Jucha* (UPM NV 15)	Cervical	69	50	61
cf. *Jucha* (UPM NV 15)	Cervical*	70.2	51	62.2
cf. *Jucha* (UPM NV 15)	Cervical*	69.8	52	63.4
cf. *Jucha* (UPM NV 15)	Cervical*	72.5	NA	64.6
cf. *Jucha* (UPM NV 15)	Cervical*	72.4	55	67.3
cf. *Jucha* (UPM NV 15)	Cervical*	75.8	NA	69.9
cf. *Jucha* (UPM NV 15)	Cervical*	74.5	58.6	70.3
cf. *Jucha* (UPM NV 15)	Cervical*	75.2	59	71.5
cf. *Jucha* (UPM NV 15)	Cervical	74.6	59	72.5
cf. *Jucha* (UPM NV 15)	Cervical*	76.9	58.6	73.7
cf. *Jucha* (UPM NV 15)	Cervical*	82	NA	NA
cf. *Jucha* (UPM NV 15)	Cervical*	81	NA	NA
cf. *Jucha* (UPM NV 15)	Cervical‡	81.5	NA	NA
cf. *Jucha* (UPM NV 15)	Cervical‡	81	NA	NA
cf. *Jucha* (UPM NV 15)	Cervical‡	81.5	NA	NA
cf. *Jucha* (UPM NV 15)	Cervical*	81.3	64.5	NA
cf. *Jucha* (UPM NV 15)	Cervical*	81	NA	NA
cf. *Jucha* (UPM NV 15)	Cervical	78.5	67.5	82.3
cf. *Jucha* (UPM NV 15)	Cervical	78.7	NA	82.7
cf. *Jucha* (UPM NV 15)	Cervical*	77.6	NA	84.4
cf. *Jucha* (UPM NV 15)	Cervical*	74.8	NA	84.7
cf. *Jucha* (UPM NV 15)	Cervical	71.5	68.9	87
cf. *Jucha* (UPM NV 15)	Cervical	74.4	NA	86.3
cf. *Jucha* (UPM NV 15)	Cervical	71	NA	NA

Specimen	Region	Length	Medial height	Width
cf. *Jucha* (UPM NV 15)	Caudal	45.6	58.1	71
cf. *Jucha* (UPM NV 15)	Caudal*	46.2	55	63.6
cf. *Jucha* (UPM NV 15)	Caudal*	44.9	55.9	60.4

***(and, when needed, ‡): Articulated series. Missing data is indicated by "NA".**

Table 2. Measurements (in millimetres) of non-axial elements of *Jucha squalea* and cf. *Jucha*

Specimen	Element	Anteroposterior length (proximally)	Anteroposterior length (distally)	Proximodistal length
Jucha squalea, holotype (UPM 2756/1-53)	Humerus	90	NA	NA
Jucha squalea, holotype (UPM 2756/1-53)	Radius	125	NA	155
Jucha squalea, holotype (UPM 2756/1-53)	Left femur	94	178	270
Jucha squalea, holotype (UPM 2756/1-53)	Right femur	95	174	269
Jucha squalea, holotype (UPM 2756/1-53)	Tibia	117	NA	101
Jucha squalea, holotype (UPM 2756/1-53)	Fibula	95	NA	105
Jucha squalea, holotype (UPM 2756/1-53)	Pedal phalange	42	NA	64
Jucha squalea, holotype (UPM 2756/1-53)	Pedal phalange	38	NA	58
Jucha squalea, holotype (UPM 2756/1-53)	Pedal phalange	40	NA	63

Specimen	Element	Anteroposterior length (proximally)	Anteroposterior length (distally)	Proximodistal length
cf. *Jucha* (UPM NV 15)	Humerus	NA	165	295

Missing data is indicated by "NA".

Table 3. Anterior cervical measurements (height, length and width; in millimetres) and position for cervical centra at or close to the position of the tenth centrum (columns 4–7) and for the relatively longest cervical centrum record (columns 8–11) (for an R-friendly version, see Supporting Information, supplementary files)

Specimen	Source	Height, centrum 10	Length, centrum 10	Width, centrum 10	Position	Height of longest centrum	Length of longest centrum	Width of longest centrum	Position of longest centrum
Holotype, MOR 751	Druckenmiller (2002), from figure	42.8	34.3	NA	10	42.8	34.3	NA	10
Holotype, GPMM A3.B4	Sachs *et al.*(2016)	25	23	NA	10	25	23	NA	10
LACM2832	Welles (1952); O' Gorman (2020)	22	27	41	12	26	37	51	20
Holotype, CMNH1588	Welles (1952)	50	56	68	10	81	123	102	35
Holotype, UCMP33912	Welles (1952)	35	50	56	12	39	65	NA	20
Holotype, UCMP38349	Welles (1962)	32	38	49	10	50	65	71	20
Holotype, AM F9644	Kear (2002b)	25.9	25.29	35.55	10	17.7	21.21	24.12	2
Holotype, QM F12219	This paper (three-dimension	50.55	69.3	70.76	NA	50.55	69.3	70.76	NA

Specimen	Source	Height, centrum 10	Length, centrum 10	Width, centrum 10	Position	Height of longest centrum	Length of longest centrum	Width of longest centrum	Position of longest centrum
	al surface scan)								
Holotype, QM F6890	Persson (1960)	45	62	58	NA	33	50	47	NA
SU01	Utsunomiya (2019)	25	35	38	10	25	35	38	10
MOZ PV 6893	O'Gorman *et al.* (2015a)	42	45	NA	NA	33	42	48	NA
MOZ PV 6890	O'Gorman *et al.* (2015a)	47	59	52	NA	46	60	51	NA
MOZ PV 6991	O'Gorman *et al.* (2015a)	60	69	NA	NA	52	63	NA	NA
SSU 104-a/17-19	Dubeikovsky & Ochev (1967)	51	62	57	NA	51	62	57	NA
YSPU1896-32	Zverkov & Kiselev (2018)	67.1	94.6	83	NA	67.1	94.6	83	NA
Holotype, SMU SMP 69120	Welles (1949)	40	52	65	13	55	95	93	30
SMNK-PAL-3978	Buchy (2005)	NA	42	NA	10	NA	42	NA	10
Holotype, BGR Ma 13328	Sachs *et al.*(2017)	43	45.72	45.53	NA	49.83	59.13	53.23	NA
AMNH1495	Otero (2016)	40.65	56.78	55.24	10	44.98	70.44	62.83	14
Holotype, AMNH5835	Otero (2016)	32.23	58.05	51.58	10	32.23	58.05	51.58	10

Specimen	Source	Height, centrum 10	Length, centrum 10	Width, centrum 10	Position	Height of longest centrum	Length of longest centrum	Width of longest centrum	Position of longest centrum
Holotype, KUVP1301	Welles (1952); Otero (2016)	60	78	NA	6	60	78	NA	6
AMNH2554	Otero (2016)	84.04	75.55	111.84	9	84.04	75.55	111.84	9
Holotype, TMP2007.011.001	Kubo *et al.*(2012)	45	70	57	25	23	38	31	3
Holotype, ANSP 10081	Sachs (2005b)	31	51	43	10	54	93	65	32
Holotype, MLP 93-I-5-1	O'Gorman *et al.* (2015b)	27	32	38	10	39	51	55	20
Holotype, MOR3072	Serratos *et al.* (2017)	30.4	34.7	48	10	31.4	40.2	51.6	13
MCS PV4 'C2'	O'Gorman (2016)	33	45	50	NA	33	45	50	NA
NZGS, CD426	Wiffen & Moisley (1986)	32	42	43	8	30	40	41	5
Holotype, MLP 40-XI-14–6	Gasparini *et al.* (2003)	53	60	96	NA	53	60	96	NA
Holotype, SGO.PV.957	Otero *et al.*(2014)	57.5	56	75.3	10	57.5	56	75.3	10
Holotype, MGUAN PA103	Araújo *et al.*(2015a), from figure	35.7	53.1	59.6	NA	35.7	53.1	59.6	NA
Holotype, RSM P2414.1	Sato (2003)	37	62	55	8	24	43	39	3
Holotype, UPM 2756/1-53	This paper	52	70.5	67	NA	52	70.5	67	NA

Specimen	Source	Height, centrum 10	Length, centrum 10	Width, centrum 10	Position	Height of longest centrum	Length of longest centrum	Width of longest centrum	Position of longest centrum
UPM NV 15	This paper	49	68.6	62	NA	49	68.6	62	NA

We computed the length-to-height ratio of each specimen and used a time-scaled, randomly selected most parsimonious tree (see above) to infer ancestral (node) values in a maximum likelihood framework, using the phytools v.0.7-10 package (Revell, 2012). We used these data to create phenograms of cervical centrum elongation throughout the evolutionary history of elasmosaurids. We also used the data from Soul & Benson (2017) to evaluate the correlation between neck length and cervical elongation in long-necked ('plesiosauromorph') plesiosaurians (Supporting Information, Table S2; supplementary files).

RESULTS: SYSTEMATIC DESCRIPTION

Sauropterygia Owen, 1860

Plesiosauria de Blainville, 1835

Xenopsaria Benson & Druckenmiller, 2014

Elasmosauridae Cope, 1869

***Jucha squalea* gen. nov., sp. nov.**

Zoobank registration:

Publication LSID: urn:lsid:zoobank.org:pub:8CF4F7E1-7DE3-46DE-ABC3-34C4597DABCC

Genus LSID: urn:lsid:zoobank.org:act:A5A9FD2C- 86CB-4CA5-A41A-22812277A226

Species LSID: urn:lsid:zoobank.org:act:8A9BDEF1- 47B6-4616-8A70-59B505DBD8FA

Etymology

The generic name comes from the Cyrillic Юха, a snake-like demon associated with water in local Volga–Ural region folklore. In English phonology, the generic name is pronounced 'you kha'. The specific name is the Latin for coated, covered, rugose, referring to the pyrite layer found on many bones of the holotype.

Holotype

UPM 2756/1-53, a disarticulated partial skeleton discovered in 2007 by a field crew led by one of us (G.N.U.), comprising 22 cervical centra, 19 dorsal centra including two pectorals, one sacral and four caudals, two partial coracoids, two partial humeri, one radius, one radiale, several metacarpals and phalanges, two complete femora, one tibia, one fibula, fragmentary ribs and gastralia. This specimen originates from the *Speetoniceras versicolor* Zone (upper Hauterivian, Lower Cretaceous) in the vicinity of the Slantsevy Rudnik village (Fig. 1), Ulyanovsk Oblast, European Russia.

Diagnosis

Jucha squalea is characterized by the following autapomorphies among Elasmosauridae: (1) strongly waisted anterior to middle dorsal centra, giving the centrum an hourglass shape in ventral view; (2) massive distally-thickening transverse processes in middle to posterior dorsal vertebrae; (3) absence of a heart-shaped intercoracoid fenestra; and (4) large radius that is anteroposteriorly longer than the humeral head/capitulum.

Jucha squalea is also characterized by a unique combination of features, the most salient of which are as follows: (1) elongated anterior cervicals, with a length-to-height ratio ≤ 1.36, similar to *Er. australis* and *Kawanectes lafquenianum* (Gasparini & Goñi 1985) (O'Gorman, 2016); (2) absence of ventral notch in all cervical centra, as in *La. richterae* (Sachs *et al.*, 2017), *Callawayasaurus colombiensis* (Welles, 1962), *Zarafasaura oceanis* Vincent *et al.*, 2011 (Lomax & Wahl, 2013; O'Gorman, 2020) and unlike *Er. australis* (V. Fischer, pers. obs.) and derived elasmosaurids (Welles, 1943, 1952; Otero, 2016; O'Gorman, 2020); (3) triangular, anteroposteriorly short anteromedial process of the coracoid, as in *Styxosaurus* (Welles & Bump, 1949; Welles, 1952; Otero, 2016), *Thalassomedon haningtoni* Welles, 1943 and *Nakonanectes bradti* Serratos *et al.*, 2017; (4) small, slit-like epipodal notch (also called radioulnar/tibiofibular foramen, spatium interosseum) in both the forelimb and the hindlimb, as in *Hydrotherosaurus alexandrae* Welles, 1943,

and *Morenosaurus stocki* Welles, 1943; and (5) large tibia that is anteroposteriorly longer than femoral head/capitulum, as in *Callawayasaurus colombiensis*(Welles, 1962).

Stratum typicum

Speetoniceras versicolor Zone of the Klimovka Formation, upper Hauterivian, Lower Cretaceous.

Locus typicus

Slantsevy Rudnik, Ulyanovsk Oblast, European Russia.

Description

The specimen UPM 2756/1-53 belongs to an osteologically mature individual, having neural arches fused with the centrum (Brown, 1981), elongated propodials (O'Keefe & Chiappe, 2011) and finished bone surfaces on girdle elements.

Cervical vertebrae:

At least 22 disarticulated cervicals are preserved in the holotype (Figs 2, 3), with no occurrence of the atlas and axis. One of these cervicals is a single, isolated anterior cervical (Fig. 3A–C; Table 1), suggesting that the neck comprised at least 24 elements (including the atlas and the axis), and probably many more. This anterior cervical centrum is markedly smaller (especially dorsoventrally) than the more posterior cervicals preserved (it is only 30 mm high and 38 mm long, compared with 43–49 mm high and 58–64 mm long for the next two smallest anterior cervicals; Table 1). Such a marked increase in centrum size along the neck is a frequent feature in derived elasmosaurids (O'Keefe & Hiller, 2006; O'Gorman *et al.*, 2015b; Sachs *et al.*, 2018) and suggests that *J. squalea* possessed several tens of cervical centra, although the precise number is impossible to estimate at present.

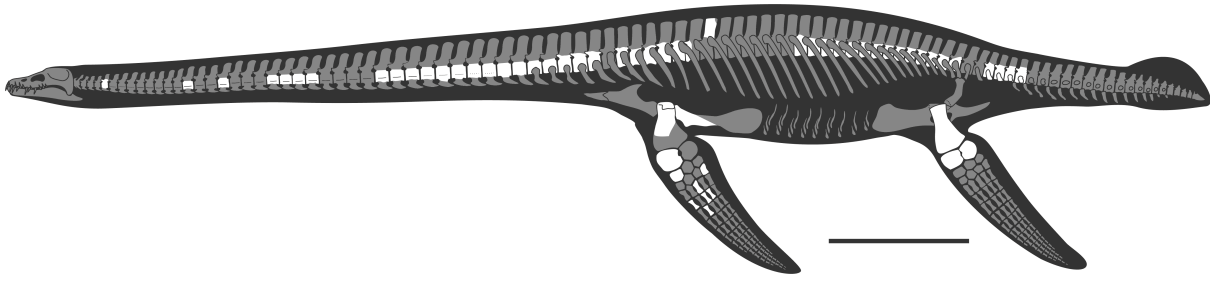

Figure 2. Skeletal reconstruction of the holotype specimen of *Jucha squalea* (UPM 2756/1-53). Preserved bones are coloured in white; the reminder of the osteology is based on *Callawayasaurus colombiensis*, *Thalassomedon haningtoni* and *Hydrotherosaurus alexandrae* (Welles, 1943, 1962).

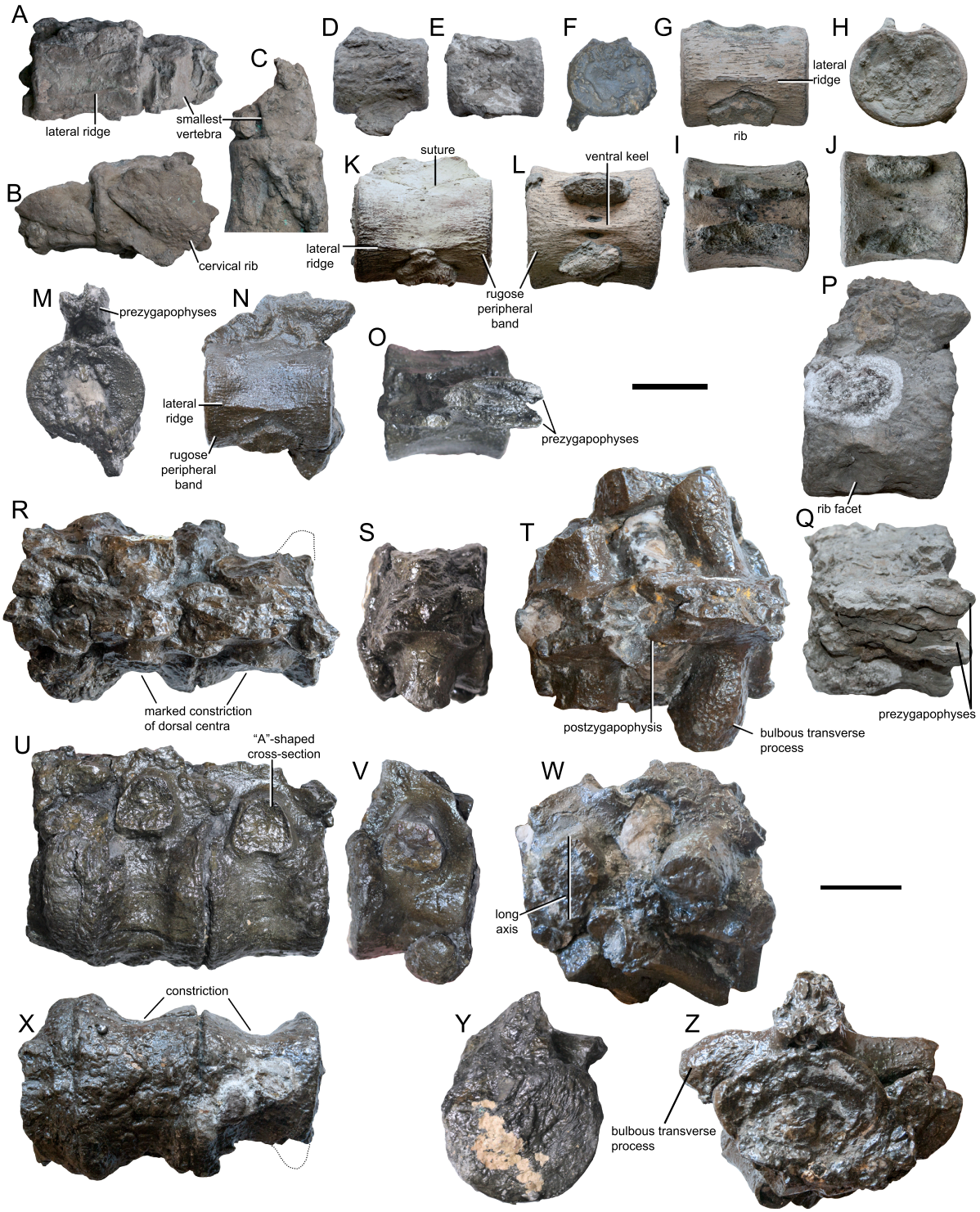

Figure 3. Cervical, pectoral and anterior dorsal vertebrae of Jucha squalea (UPM 2756/1-53). A–C, smallest preserved anterior cervical vertebrae in lateral view (A, B) and

articular surface of the smallest preserved vertebra (C). D–O, anterior to middle cervical vertebrae in lateral (D, G, K, N), ventral (E, L, J), articular (F, H, M) and dorsal (I, O) views. P, Q, posterior cervical vertebra in right lateral (P) and dorsal (Q) views. R–Z, pectoral to anterior dorsal vertebrae in dorsal (R–T), right lateral (U–W), ventral (X) and articular (Y, Z) views. Scale bars: 50 mm.

The cervical vertebrae are elongated; their length-to-height ratio is between 0.95 (posteriormost cervicals) and 1.36 (occurring in the anterior third of the neck). The anterior cervical centra are clearly elongated, approaching the 'can-shaped' condition (Fig. 3A–O; Tables 1 and 3). This shape resembles that of *Er. australis* and differs from many Early Cretaceous elasmosaurids that have less elongated cervical centra, such as *Callawayasaurus colombiensis* (Welles, 1962) and *La. richterae* (Sachs *et al.*, 2017) (Table 3). The cervical centra of *J. squalea*are also more elongated than in *N. bradti* (Serratos *et al.*, 2017) and many weddellonectian euelasmosauridans for which this feature is known (Tables 3).

The articular surfaces are oval in outline, with their dorsal margin depressed under the neural canal (Fig. 3F, H, M). The ventral edge of the articular surface is continuously rounded, unlike derived elasmosaurids, in which a ventral notch gives the articular surface a binocular shape (O'Keefe, 2001); such a depression is also present but faint in *Er. australis* (V. Fischer, pers. obs. on holotype QMF11050). The articular surfaces are essentially platycoelous; they are amphicoelous in *La. richterae*, *Albertonectes vanderveldei* Kubo *et al.*, 2012, *Libonectes morgani* (Welles, 1949) and *Th. haningtoni* (Kubo *et al.*, 2012; Sachs & Kear, 2015; Sachs *et al.*, 2017). The central part of the articular surface is slightly concave, lacking the central boss observed in the indeterminate Hauterivian elasmosaurid SSU 104-a/17 (Dubeikovsky & Ochev, 1967). In all of the preserved cervical centra, there are no ventral protrusions (lips), in contrast to SSU 104-a/17 (Dubeikovsky & Ochev, 1967) and possibly *La. richterae* (Sachs *et al.*, 2017).

A consistent feature of *J. squalea* is the presence of a strongly rugose peripheral band adjacent to the articular surface of cervical centra, forming irregular, anteroposteriorly oriented ridges and furrows on the lateral and, to a lesser degree, ventral surfaces of the centrum (Fig. 3G, K, L, N). A peripheral rugosity in vertebral centra is variably present in many adult plesiosaurians (e.g. Owen, 1840; Seeley, 1874), including other Hauterivian specimens from France (Fournier *et al.*, 1982) and the UK (the Speeton plesiosaur; N. G. Zverkov, pers. obs. on NHMUK PV R8623, April 2019), but it appears much more pronounced and consistently restricted to all cervical–pectoral centra. In contrast, rugosities appear entirely absent in SSU 104-

a/17 (Dubeikovsky & Ochev, 1967) and *La. richterae* (Sachs *et al.*, 2017) and are present but faint in *Callawayasaurus colombiensis* (Welles, 1962).

Cervical centra are slightly waisted. Paired oval foramina are present on the ventral side and are separated by a rounded median keel, as in all elasmosaurids. The cervical rib facets are lozenge shaped anteriorly and become rounded posteriorly (Fig. 3G, N, P). A sharp lateral, anteroposteriorly oriented ridge [a feature frequently evolved convergently among long-necked plesiosaurians (e.g. Noè, *et al.*, 2017; Fischer *et al.*, 2018)] is present immediately dorsal to the rib facet in anterior and middle cervical centra (Fig. 3A, G, K, N). Posterior cervicals lack this feature (Fig. 3P). The prezygapophyses are mediodistally narrow and face dorsomedially. They are separated from one another from at least one-third of their length (Fig. 3O). No neural spine is preserved. All the preserved neural arches are fully fused to their corresponding centra; the suture is V-shaped in lateral view (Fig. 3K).

Pectoral and dorsal vertebrae:

Four and a half vertebrae from the pectoral to anterior dorsal region are preserved (Fig. 3R–Z), in addition to a complete and articulated mid-dorsal to sacral series (Fig. 4). Anterior to middle dorsal centra are markedly waisted transversely, giving the centrum an hourglass shape in ventral view (Figs 3R, X, 4C, F). Pectoral centra are wider than high, and the dorsal centra become progressively as wide as high and then slightly higher than wide throughout the dorsal series.

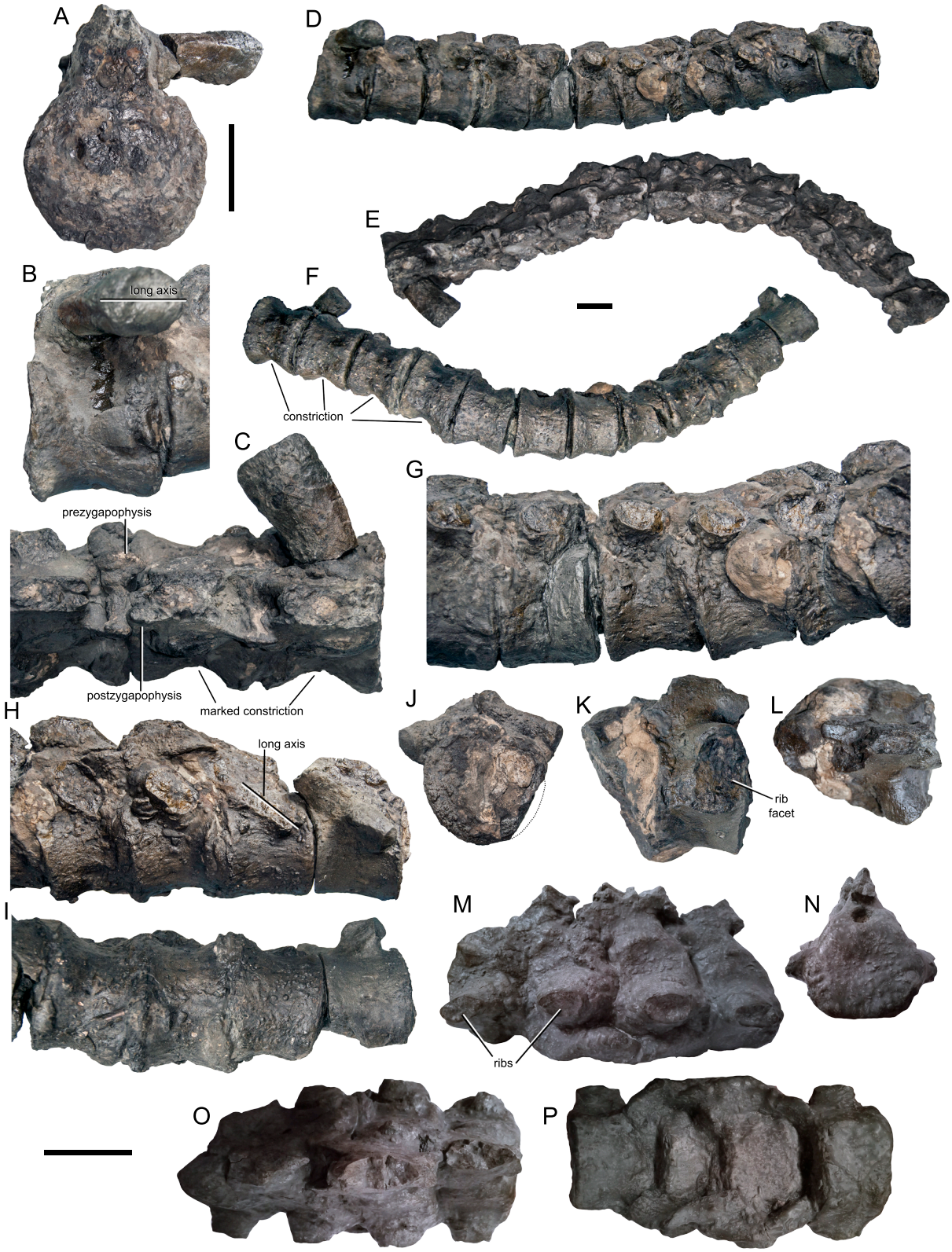

Figure 4. Dorsal, sacral and caudal vertebrae of *Jucha squalea* (UPM 2756/1-53). A–C, middle dorsal vertebra in anterior (A), left lateral (B) and dorsal (C) views. D–F, articulated middle to posterior dorsal vertebrae in left lateral (D), dorsal (E) and ventral (F) views. G, H, magnified regions of (A), dorsal vertebra in lateral view. I, J, posterior-most dorsal vertebrae in ventral (I) and posterior (J) views. K, L, sacral vertebra in left

lateral (K) and dorsal (L) views. M–P, articulated caudal vertebrae in left lateral (M), posterior articular (N), dorsal (O) and ventral (P) views. Scale bars: 50 mm.

Another peculiar feature of *J. squalea* is the robust, distally thickening transverse processes in the middle to posterior dorsal region (Fig. 4A, C). The orientation of the long axis of the distal end of these processes varies throughout the dorsal series; it is oriented dorsoventrally in the pectorals (Fig. 3W) and almost horizontally in the midposterior dorsals (Fig. 4B), before progressively orienting posteroventrally in the posteriormost dorsals (Fig. 4H). This condition somewhat resembles that of the dorsoventrally flattened *Tatenectes laramiensis* (Knight, 1900) (O'Keefe *et al.*, 2011). The transverse processes in pectorals and anterior dorsals have a shallow ventral groove, giving the process an 'A'-shaped cross-section (Fig. 3U); a similarly placed but much deeper 'subdiapophyseal fossa' has been reported in '*Gronausaurus wegneri*' Hampe, 2013 [= *Brancasaurus brancai* according to Sachs *et al.*(2016)]. In the posteriormost dorsals, the transverse processes abruptly become compressed, with a rectangular cross-section.

These posterior dorsal centra are also not waisted, unlike the previous ones, which have the autapomorphic hourglass shape in ventral view (Fig. 4F). Paired ventral foramina are present and positioned ventrolaterally throughout the dorsal series. The prezygapophyses are strongly concave, with a dorsomedial concavity; they progressively separate from one another throughout the dorsal series, becoming separated over at least one-half of their length in posterior dorsals (Fig. 4C).

An isolated, fragmentary neural spine is present; this fragment is 100 mm high and mediolaterally thickens dorsally, suggesting that it originates from the dorsal region. This fragment indicates that dorsal neural spines were substantially higher than their corresponding centra, because none of the preserved centra exceeds 82 mm in dorsoventral height. A similar condition is present in one of the Speeton plesiosaurians, NHMUK PV R8623 (N. G. Zverkov, pers. obs. April 2019), and in an indeterminate Hauterivian specimen from France (Fournier *et al.*, 1982).

Sacral and caudal vertebrae:

One sacral vertebra is preserved. The base of the transverse process is large again, and its long axis is vertical (Fig. 4K). The sacral centrum is similar to the posteriormost dorsals in being unwaisted ventrally. Paired foramina are present and positioned ventrolaterally.

A series of four caudal vertebrae with articulated ribs and neural arches is preserved. The caudal vertebrae are anteroposteriorly short (Fig. 4M, P). The articular surfaces are oval to subhexagonal in outline, with the width exceeding the height (Fig. 4N). The caudal ribs are thick and become dorsoventrally compressed posteriorly.

Ribs:

Anterior cervical ribs have a lozenge-shaped basal cross-section (Fig. 3B, D, L); their cross-section becomes progressively oval, then circular along the cervical series. Distally, the anterior cervical rib forms a small, pointed, proximally placed anterior process and a longer posterodistal process (Fig. 3B), resembling those of *Futabasaurus suzuki* Sato, Hasegawa, & Manabe, 2006 and, possibly, *Callawayasaurus colombiensis* (Welles, 1962). This differs from elasmosaurids that have 'hatchet'-shaped cervical ribs, where the anterior and posterior processes are placed distally [e.g. *Albertonectes vanderveldei* (Kubo *et al.*, 2012), *Styxosaurus browni* (Otero *et al.*, 2016) and *Elasmosaurus platyurus*Cope, 1868 (Sachs, 2005b)].

Coracoid:

Both coracoids are preserved in connection but are fragmentary (Fig. 5A–F). The coracoid symphysis is thickened ventrally (215:1) and slightly thickened dorsally, giving it an eye shape in medial view, with a median ventral protrusion (Fig. 5D). This ventral protrusion is moderately pronounced, as in *Callawayasaurus colombiensis* (Welles, 1962), and unlike the extremely protruding process of *Wa. betsynichollsae* (Druckenmiller & Russell, 2006) and *Li. morgani* (Sachs & Kear, 2017). The symphysis is undulating in ventral view and is bordered by thin anteroposterior ridges texturing the bone surface. The dorsal and ventral surfaces of the coracoid are flattened, and the dorsal surface essentially lacks a mediolateral buttress (Fig. 5D, E). A slight swelling is present on the anterior portion but does not result in an anterior depression; therefore, we scored this character as 214:2.

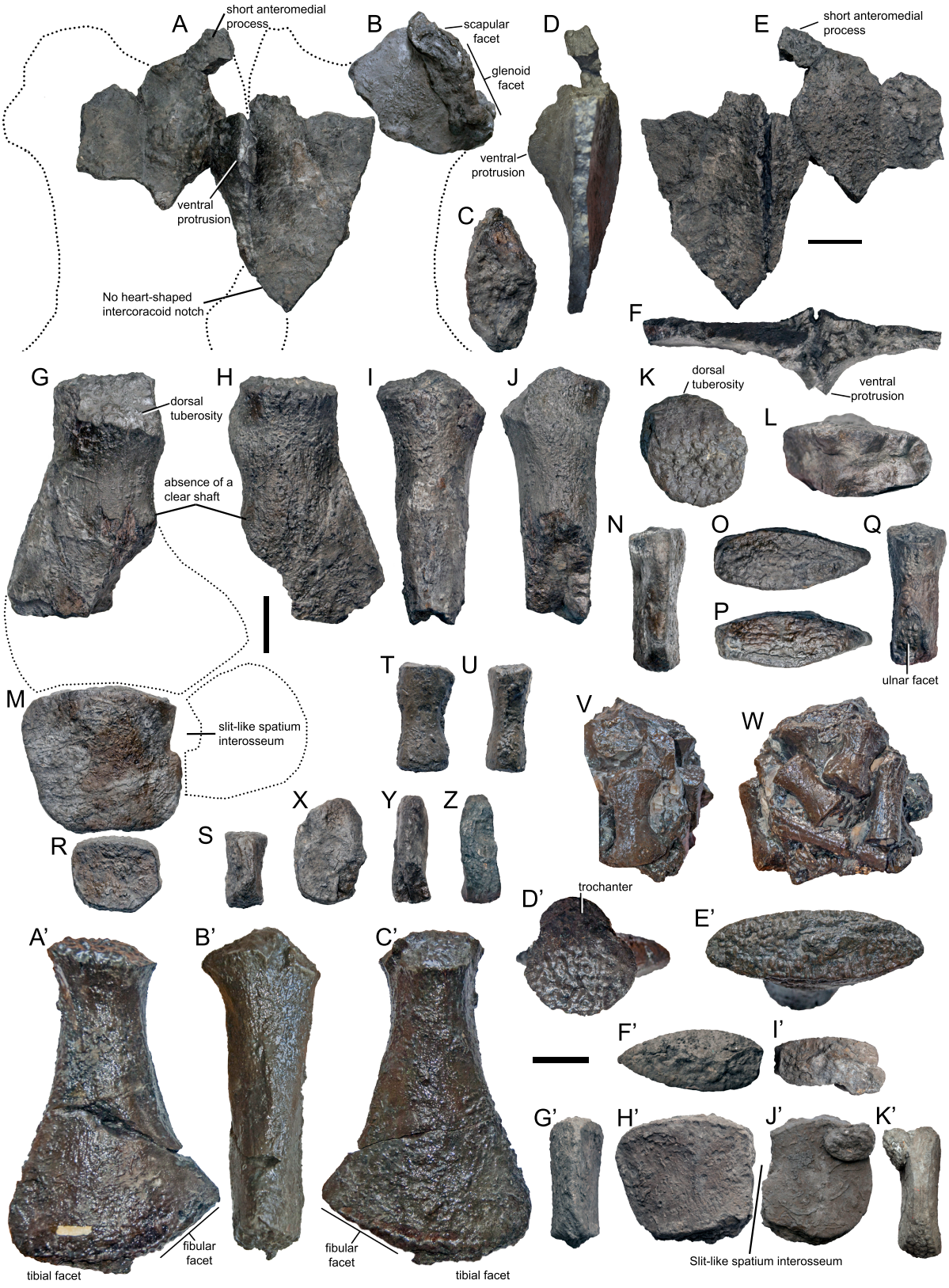

Figure 5. Appendicular skeleton of *Jucha squalea* (UPM 2756/1-53). A–F, articulated coracoids in ventral (A, B), lateral (D), dorsal (E) and anterior (F) views; C, articular view of glenoid portion. G–L, partial left humerus in dorsal (G), ventral (H), anterior (I), posterior (J), proximal (K) and distal (L) views. M–Q, radius in dorsal (M), anterior (N), proximal (O), distal (P) and posterior (Q) views. R, S, radiale in dorsal (R) and anterior

(S) views. T, U, metacarpal or proximal phalanx. V, W, phalanges; X–Z, fifth metacarpal in dorsal (X), posterior (Y) and anterior (Z) views. A′–E′, right femur in ventral (A′), posterior (B′), dorsal (C′), proximal (D′) and distal (E′) views. F′–H′, left tibia in proximal (F′), anterior (G′) and dorsal (H′) views. I′–K′, left fibula in proximal (I′), dorsal (J′) and posterior (K′) views. Scale bars: 50 mm.

The anteromedial process is preserved; its anterior and medial surfaces are thickened and concave, whereas its anterolateral edge is thin and sheet-like. The anteromedial process is anteroposteriorly short and triangular in outline; the medial surfaces of the anteromedial processes are divergent, and the angle formed by the medial and anterolateral margins of the anteromedial process is ~65° in *J. squalea* (Fig. 5A, E). *Styxosaurus* spp., *Th. haningtoni* and *H. alexandrae* have an angle >50° (Welles, 1943, 1952; Welles & Bump, 1949), whereas it is only ~40° in *Callawayasaurus* and *Aphrosaurus furlongi* Welles, 1943 (Welles, 1943 (Welles, 1962, O'Gorman, 2020) and ~35° in *Wa. betsynichollsae* (Druckenmiller & Russell, 2006). The anteromedial process is located close to the ventral protrusion, indicating a weak development of the pectoral bar (Fig. 5A, D). This condition resembles that of *Styxosaurus* (Welles & Bump, 1949; Welles, 1952; Otero, 2016), *Th. haningtoni* (Welles, 1943) and, to a certain degree, *N. bradti* (Serratos *et al.*, 2017) but differs from many other elasmosaurids, whose anteromedial processes protrude far more anteriorly (Welles, 1962; Druckenmiller & Russell, 2006; Araújo *et al.*, 2015a; Sachs *et al.*, 2017; O'Gorman, 2020).

The medial surfaces of the coracoids diverge gradually posterior to the symphysis (Fig. 5A); the preserved portions of the coracoids suggest that *J. squalea* lacks a posteromedial process, which forms the heart-shaped intercoracoid cavity seen in all known elasmosaurids (e.g. Welles, 1943, 1952, 1962; Druckenmiller & Russell, 2006; Otero, 2016; O'Gorman, 2020). The angle between the scapular and glenoid facets is ~150°; they are poorly demarcated and have an irregularly papillose surface (Fig. 3B, C). The coracoid of *J. squalea*thus lacks several features of other known basal elasmosaurids.

Humerus:

Only the proximal parts of both humeri are preserved. The humerus appears robust (Fig. 5G). Its anteroposterior width rapidly increases distally from the proximal end, resulting in a basically unwaisted shaft, resembling that of *F. suzuki* (Sato *et al.*, 2006) and unlike that of most other elasmosaurids (e.g. Welles, 1943, 1952, 1962; Otero, 2016; O'Gorman, 2020). In this aspect, the humerus exhibits similarities to some aristonectines that have paedomorphic limbs (e.g. Araújo *et al.*, 2015b), although the limbs of *J.*

squalea do not show any marked evidence of a delayed or slowed ossification. The humeral head (capitulum) and dorsal tuberosity are not separated by the band of periosteal bone, unlike *H. alexandrae* and *Mo. stocki* (Welles, 1952). Their surfaces are flattened and irregularly papillate, indicating the presence of an extensive cartilaginous cap *in vivo*. The dorsal tuberosity is as wide anteroposteriorly as the humeral head and is deflected postaxially (Fig. 5K).

Radius:

The radius of *J. squalea* is unique in being large, markedly longer anteroposteriorly than the head of the humerus. The humeral facet is oval, rugose and slightly convex (Fig. 5M). The anterior edge is straight and anteriorly tapering and is made of finished bone (Fig. 5N). The posterior facet of the radius is bifid, because of the presence of a median concavity forming the anterior edge of the radioulnar foramen (Fig. 5M, Q). A radial notch is thus present, but the contribution of the radius to the radioulnar foramen is small, as in *H. alexandrae*, *Mo. stocki* and *Aphrosaurus furlongi* (Welles, 1952; O'Gorman, 2020) but unlike '*Gronausaurus wegneri*' (Hampe, 2013), *Callawayasaurus colombiensis* (Welles, 1962) and several derived elasmosaurids (Welles, 1949, 1952; Sato *et al.*, 2006; Otero *et al.*, 2014; Hiller *et al.*, 2017). Proximally, the articulation with the ulna is barely noticeable and possibly absent, unlike '*Gronausaurus wegneri*' [= *Brancausaurus brancai* according to Sachs *et al.*(2016)] and many elasmosaurids (Welles, 1962; Hampe, 2013; O'Gorman, 2020). The radius simply forms a flattened, oblique surface (Fig. 5Q). On the contrary, the distal ulnar facet is prominent and bordered by a sharp, raised edge. A facet for the intermedium is present, but it is markedly smaller than the radiale facet and is poorly demarcated from it; this condition (character state 263.2) appears rare, being restricted to some aristonectines and *J. squalea*(Otero *et al.*, 2014; Araújo *et al.*, 2015b).

Radiale:

The radiale is thick and anteriorly tapering and possesses four articular facets for the humerus, intermedium, distal carpal 2 + 3 and distal carpal 1 (Fig. 5R). The radiale is much smaller than the radius (anteroposterior length of 77 mm, compared with 125 mm for the radius). Contrary to the radius, the anterior surface of the radiale lacks finished bone (Fig. 5S).

Metacarpal V:

A proximodistally elongated, ear-shaped element is interpreted here as the metacarpal V. This tapers posteriorly and possesses a small posterior notch

(Fig. 5X, Y). The distal facet is flat and thick, whereas the ulnare facet is triangular and anteromedially facing.

Femur:

The femur is short and robust. Like the humerus, the femur is not waisted; it starts expanding anteroposteriorly distal to the first third of total femoral length (Fig. 5A′, C′). This condition is similar to *Callawayasaurus colombiensis* (Welles, 1962; O'Gorman, 2020) and *Mo. stocki* (Welles, 1952) and differs from the longer shafts seen in '*Gronausaurus wegneri*' (Hampe, 2013), *La. richterae*(Sachs *et al.*, 2017), *Th. haningtoni*, *H. alexandrae*, *Aphrosaurus furlongi*(Welles, 1952; O'Gorman, 2020), *F. suzuki* (Sato *et al.*, 2006), '*Woolungasaurus glendowerensis*' (Elasmosauridae indet.) (Persson, 1960; Sachs, 2004) and a Hauterivian specimen from France (Fournier *et al.*, 1982); the condition appears somewhat variable in *Styxosaurus* spp. (Welles, 1952; Otero, 2016). The femur appears straight in anteroposterior and dorsoventral views and is therefore not sigmoid (Fig. 5A′–C′), although a slight diagenetic flattening cannot be ruled out. The long axis of the femur is slightly deflected posterodistally, but a marked postaxial deflexion is absent, unlike the femur in *Styxosaurus* spp., where the posterior expansion is longer (Welles, 1952, 1962). This condition appears similar to that of *Callawayasaurus colombiensis* (Welles, 1962; O'Gorman, 2020), although the anterodistal surface is less rounded than in *J. squalea*. The dorsal trochanter is thick, semicircular in cross-section, and slightly narrower (anteroposteriorly) than the femoral head (Fig. 5D′). There is no separation of the dorsal trochanter from the femoral head by periosteal bone, unlike in *Mo. stocki* (Welles, 1952) and, to smaller extent, *Callawayasaurus colombiensis*(Welles, 1962). The distal surface is rounded in dorsoventral view, making the distal facets hardly discernible, as in *Callawayasaurus colombiensis* (Welles, 1962).

Tibia:

The tibia resembles the radius in being anteroposteriorly longer than its corresponding propodial proximal head; this condition is shared only with *Callawayasaurus colombiensis* (Welles, 1962). The tibia is large and bulky; a posterior notch is present, but it is so small that it is invisible in dorsoventral view (Fig. 5H′). This condition again resembles that of *Callawayasaurus colombiensis* (Welles, 1962), although the tibial contribution appears even more reduced in *J. squalea*.

Fibula:

The fibula is rounded and slightly smaller than the tibia (Fig. 5I′–K′). The fibula possesses a small anterior notch, unlike the fibula in *Th. haningtoni*, *Aphrosaurus furlongi* and *Styxosaurus* sp. (Welles, 1962; Otero, 2016; O'Gorman, 2020). As a result, the tibioulnar foramen is small and slit-like, resembling but smaller than those of *Callawayasaurus colombiensis*, *H. alexandrae* and *Mo. stocki* (Welles, 1943, 1962), in addition to that of an indeterminate Hauterivian elasmosaurid from France (Fournier *et al.*, 1982).

Cf. *Jucha*

Referred specimens

UPM NV 15, a fragmentary disarticulated skeleton comprising 29 cervicals, at least three caudals, cervical and dorsal ribs, a partial left humerus, one epipodial element and several phalanges. This specimen originates from the *Simbirskites decheni* Zone (upper Hauterivian, Lower Cretaceous) of the Polivno locality (Fig. 1), Ulyanovsk Oblast, European Russia.

YKM 65729 + 66119, a fragmentary disarticulated skeleton comprising one cervical, ?three pectorals, 17 dorsal and two caudal vertebrae, many ribs, one partial femur, ischium and pubis. This specimen also originates from the *Simbirskites decheni* Zone (upper Hauterivian, Lower Cretaceous) of the Polivno locality (Fig. 1), Ulyanovsk Oblast, European Russia.

Preliminary note

Although these specimens are generally similar and compatible with the holotype of *J. squalea* (in addition to being spatiotemporally close), their incompleteness and poor overlap with the holotype does not allow an unambiguous referral to the same species. We therefore describe them as cf. *Jucha*, focusing our efforts on the differences from the holotype of *J. squalea*.

Description

Cervical vertebrae:

A total of 29 partly articulated cervical centra are preserved in UPM NV 15, including some from the anterior half of the neck. The anterior cervical centra of UPM NV 15 are elongated, with a length-to-height ratio reaching 1.4. Peripheral ridges and furrows appear more rugose than in the holotype of *J. squalea*, forming a pitted texture (Fig. 6A, E). The lateral ridge is either absent or present but is fainter and anteroposteriorly shorter in UPM NV 15 than in the holotype of *J. squalea*. A partial cervical rib is preserved in UPM

NV 15 (Fig. 6I–K). It bears several mediolateral ridges on its proximal part and has a longer shaft than in the ribs preserved in the holotype of *J. squalea*.

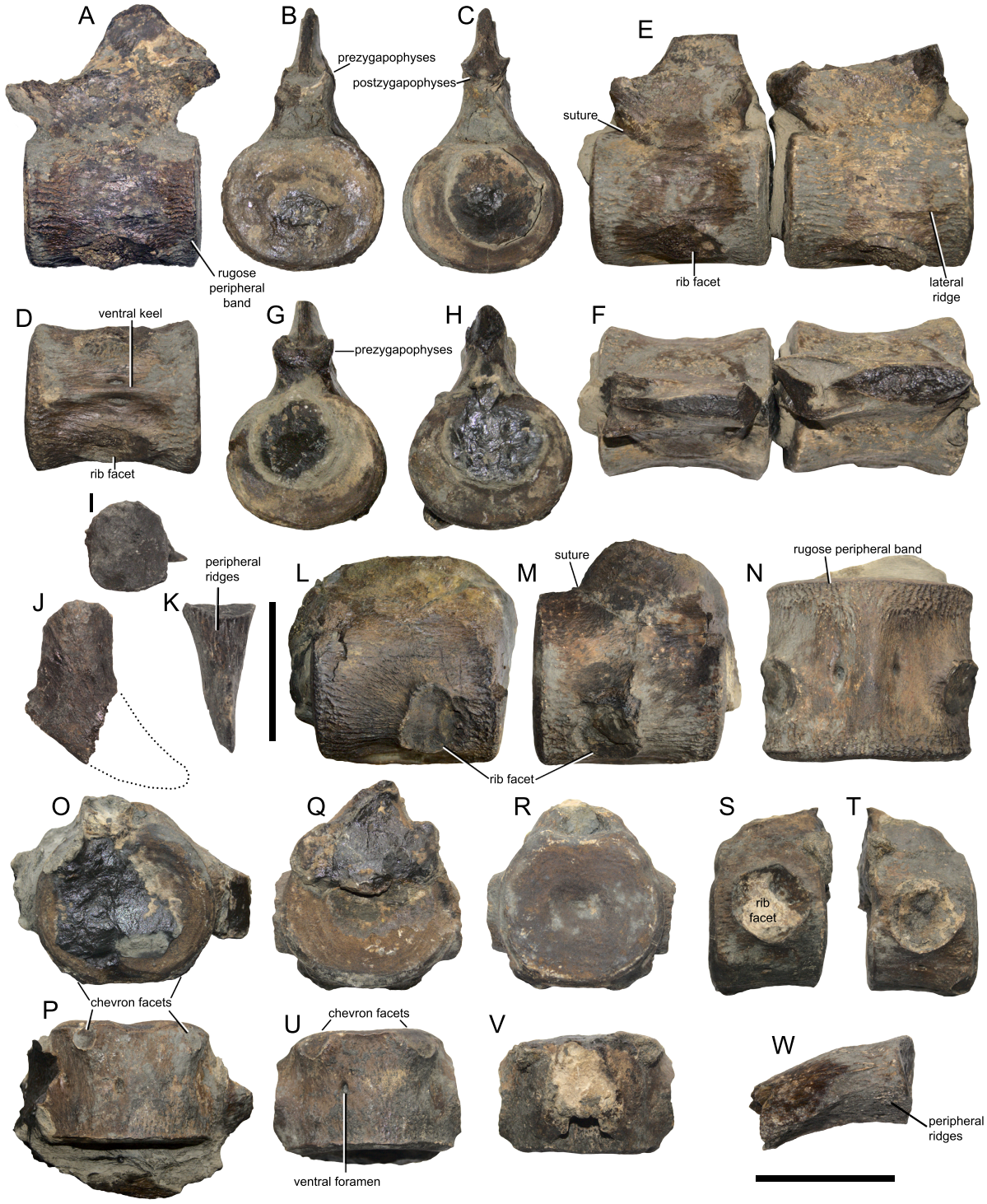

Figure 6. Axial skeleton of cf. *Jucha* UPM NV 15. A–D, anterior to middle cervical vertebra in left lateral (A), anterior (B), posterior (C) and ventral (D) views. E–H, two articulated anterior to middle cervical vertebrae in lateral (E), dorsal (F), anterior (G) and posterior (H) views. I–K, posterior cervical rib in proximal (I), dorsal (J) and posterior (K) views. L–N, posterior cervical centra in lateral (L, M) and ventral (N) views. O, P,

caudal centrum in posterior (O) and ventral (P) views; Q–T, caudal centrum in anterior (Q), posterior (R), lateral (S, T), ventral (U) and dorsal (V) views. W, proximal portion of dorsal rib. Scale bars: 50 mm.

Pectoral and dorsal vertebrae and ribs:

Three pectorals are preserved in YKM 65729 + 66119. These centra also possess the rugose peripheral band, although it appears less conspicuous than in the cervical centra of the other specimens (Fig. 7G). The dorsal neural spine is longer than the dorsoventral height of their corresponding centrum (125 vs. 79 mm; Fig. 7A, I). The dorsal surface of the dorsal neural spines is not expanded and bears a flat surface that is convex in lateral view (Fig. 7B, I, K). Dorsal transverse processes of YKM 65729 + 66119 appear more slender than in the holotype of *J. squalea* and are markedly inclined dorsolaterally (Fig. 7B, I, J); their rib facets have an oval outline, with their long axis set almost vertically. The dorsal ribs are thick, with an oval cross-section. They have a weakly sigmoidal profile in anteroposterior view: medially, the dorsal surface curves dorsolaterally and then curves ventrolaterally, as in *Albertonectes vanderveldei*and unlike '*Gronausaurus wegneri*' (Kubo *et al.*, 2012; Hampe, 2013). The ribs of UPM NV 15 bear several deep longitudinal ridges proximally but lack a posterior sulcus, unlike the ribs of '*Gronausaurus wegneri*' (Hampe, 2013).

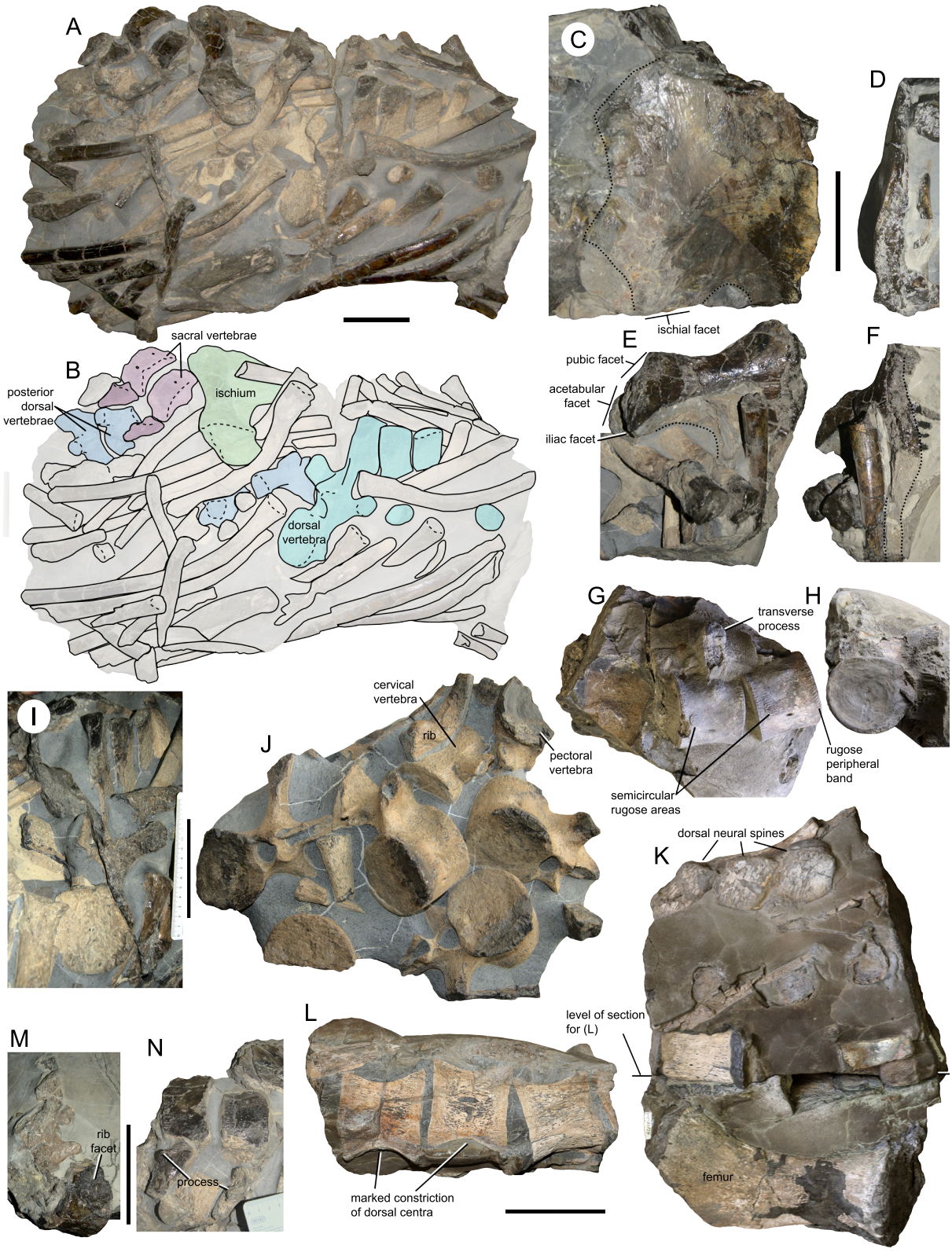

Figure 7. Axial and appendicular skeleton of cf. *Jucha* YKM 65729 + 66119. A, B, main block with vertebrae, ribs and pelvic girdle elements. C, D, left pubis in dorsal (C) and medial (D) views. E, F, left ischium in dorsal (E) and medial (F) views. G, H, pectoral vertebrae in left lateral (G) and posterior (H) views. I, mid-dorsal vertebra in posterior view. J, association of dorsal, cervical and pectoral vertebrae and ribs. K, concretion enclosing dorsal vertebrae and femur; L, cross-section of the same concretion. M,

sacral vertebra in lateral view, N, sacral vertebrae and articulated ribs in ventral view. Scale bars: 100 mm.

Sacral and caudal vertebrae and ribs:

Two vertebrae of YKM 65729 + 66119 are interpreted as sacrals (but might be anteriormost caudal, lacking chevron facets). These vertebrae are anteroposteriorly short and are preserved with their articulated ribs (Fig. 7B, N). The ventral surface is flat to slightly concave and is rugose. The rib facets are large and oval in outline, deeply concave and occupying most of the dorsoventral height of the centrum (Fig. 7M). The associated ribs are robust and expand distally; they bear a protruding, posteroventrally projecting median ventral processes (Fig. 7N).

Three caudal vertebrae are preserved in UPM NV 15. Their centra are anteroposteriorly short. The chevron facets are semi-oval and contact the posterior edge of the centrum, whereas there are no traces of chevrons on the anterior edge (Fig. 6P, U). No ventral or lateral keel is present.

Forefin:

A nearly complete left humerus is preserved UPM NV 15, in addition to a fragmentary epipodial element and numerous phalanges (Fig. 8A–K). The humerus differs slightly from that of the holotype of *J. squalea* in having a longer shaft and a more pronounced waist. The anterior surface of the humerus is essentially straight, whereas the posterior margin is strongly convex (Fig. 8A, C); the humerus appears slightly sigmoidal, bearing similarities to those of *Callawayasaurus colombiensis* and *Mo. stocki* (Welles, 1962). The radial facet faces distally, whereas the ulnar facet is deflected, facing posterodistally. This condition also resembles those of *Callawayasaurus colombiensis* and *Mo. stocki*(Welles, 1962). The dorsal tuberosity is shifted postaxially, as in the holotype of *J. squalea*. The fragmentary epipodial element lacks its posterior and distal surfaces; therefore, its absolute and relative sizes are unknown (Fig. 8F). The contribution to the radioulnar foramen is preserved, but it is difficult to assess its shape unambiguously. The proximal surface is convex and oval in outline (Fig. 8G). Phalanges are elongated and oval in cross-section.

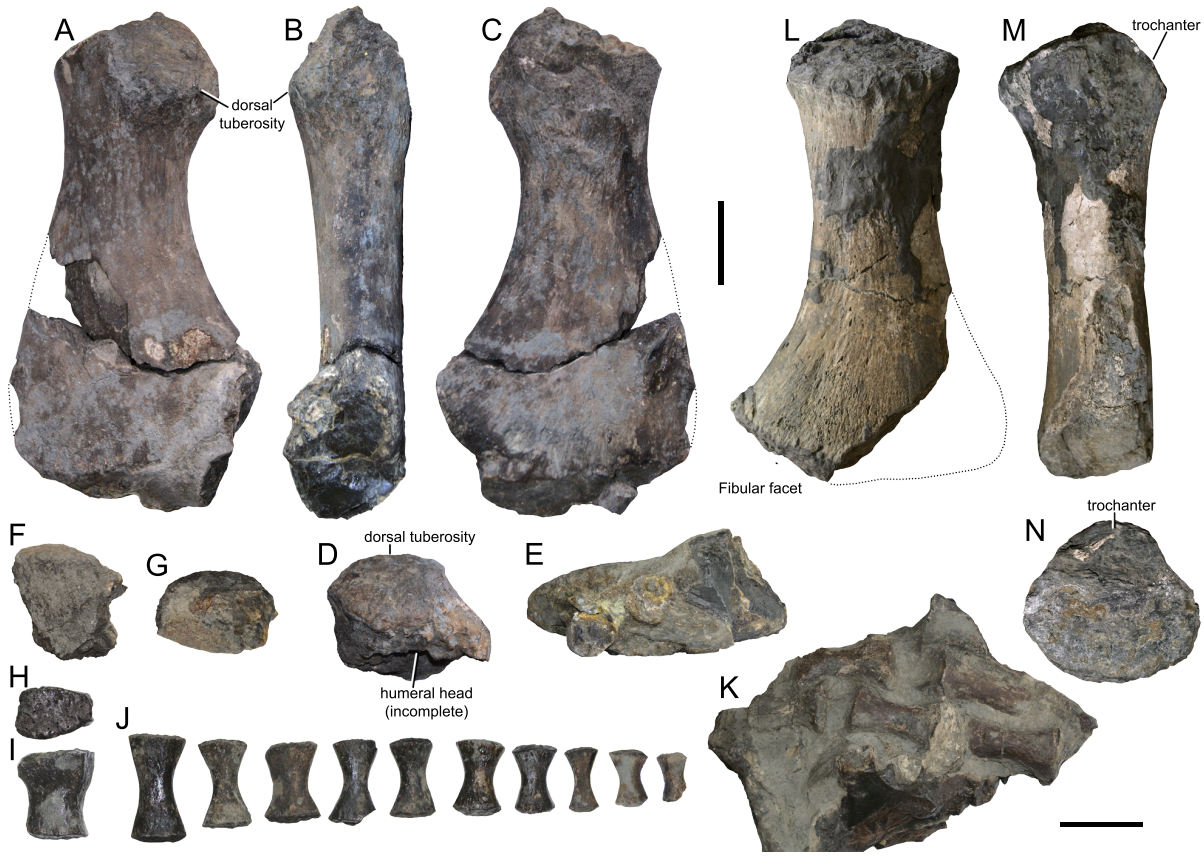

Figure 8. Appendicular skeleton of cf. *Jucha*. A–K, UPM NV 15, partial forelimb. A–E, left humerus in dorsal (A), posterior (B), ventral (C), proximal (D) and distal (E) views. F, G, partial epipodial element in dorsal or ventral (F) and proximal (G) views. H, I, possible first metacarpal in proximal (H) and dorsal (I) views. J, isolated phalanges. K, articulated phalanges in concretion. L–N, left femur of YKM 65729 + 66119 in ventral (L), anterior (M) and proximal (N) views. Scale bars: 50 mm.

Pubis:

A complete pubis is preserved in YKM 65729 + 66119 but partly obscured by matrix and other elements. The pubis has a squared outline, being as mediolaterally wide as it is anteroposteriorly long, as in other elasmosaurids (e.g. Welles, 1952). The acetabular portion is covered by matrix (Fig. 7C). The ventral surface is slightly convex, and the medial symphysis is dorsoventrally compressed and sigmoidal (Fig. 7D).

Ischium:

The left ischium is almost completely preserved in YKM 65729 + 66119, but most of the ischial blade is obscured by ribs. The ischium appears nearly as wide as long and is hatchet shaped (Fig. 7B, E). The anterior margin is shallowly concave, and the anteromedial process is short and ventrally curving, indicating the absence of a pelvic bar, unlike *El. platyurus*, *Li. morgani* and *Ka. lafquenianum* (Welles, 1943, 1952; O'Gorman,

2016; Sachs & Kear, 2017). The acetabular head is gracile, being weakly expanded anteroposteriorly (the ratio of the ischial neck-to-acetabular process length is ~0.8). The iliac and acetabular facets are poorly demarcated from the large, anteriorly facing facet for the articulation with the pubis; the acetabular contribution of the ischium appears small compared with the pubic facet (Fig. 7E). The ischium forms an anterior buttress connecting the acetabular head and the dorsomedial process. This buttress gives the ischial symphysis a sigmoid shape (Fig. 7F).

Femur:

A partial left femur is preserved in YKM 65729 + 66119. The femoral head of YKM 65729 + 66119 is massive and subcircular in outline, whereas it is dorsomedially flattened in the holotype of *J. squalea*. The dorsal trochanter is weakly expressed; its proximal surface makes an angle of ~110° with the proximal surface of the femoral head, as in UPM 2756/1-53. The trochanter is clearly narrower anteroposteriorly than the femoral head and is slightly inclined anteriorly (Fig. 8N). Although the femoral size is close to that of the holotype of *J. squalea*, it differs in the presence of a long shaft; the maximal constriction is set at midlength, whereas the maximal constriction is much more proximal in the holotype of *J. squalea* (cf. Figs 5A′, 8L). As a result, the distal expansion is restricted to the distal third of the femur, unlike in the holotype of *J. squalea* and the holotype of *Callawayasaurus colombiensis*, where its starts more proximally [this is less clear in the referred specimen of *Callawayasaurus colombiensis*(Welles, 1962); this feature might thus be variable intraspecifically]. The femur is straight in anteroposterior view, lacking any evidence for a dorsal deflection.

Phylogenetic placement

Our implied weighting maximum parsimony analyses recovered 100.000+ most parsimonious trees, with a length of 146.62811 steps. The equal weight analysis recovered 100.000+ most parsimonious trees, with a length of 1842 steps. The general structure of the strict consensus trees (Fig. 9; Supporting Information, Figs S1, S2) and the composition of the major plesiosaurian clades do not differ from those obtained in previous iterations of the dataset (Benson & Druckenmiller, 2014; Fischer *et al.*, 2018; O'Gorman, 2020) and will not be discussed here.

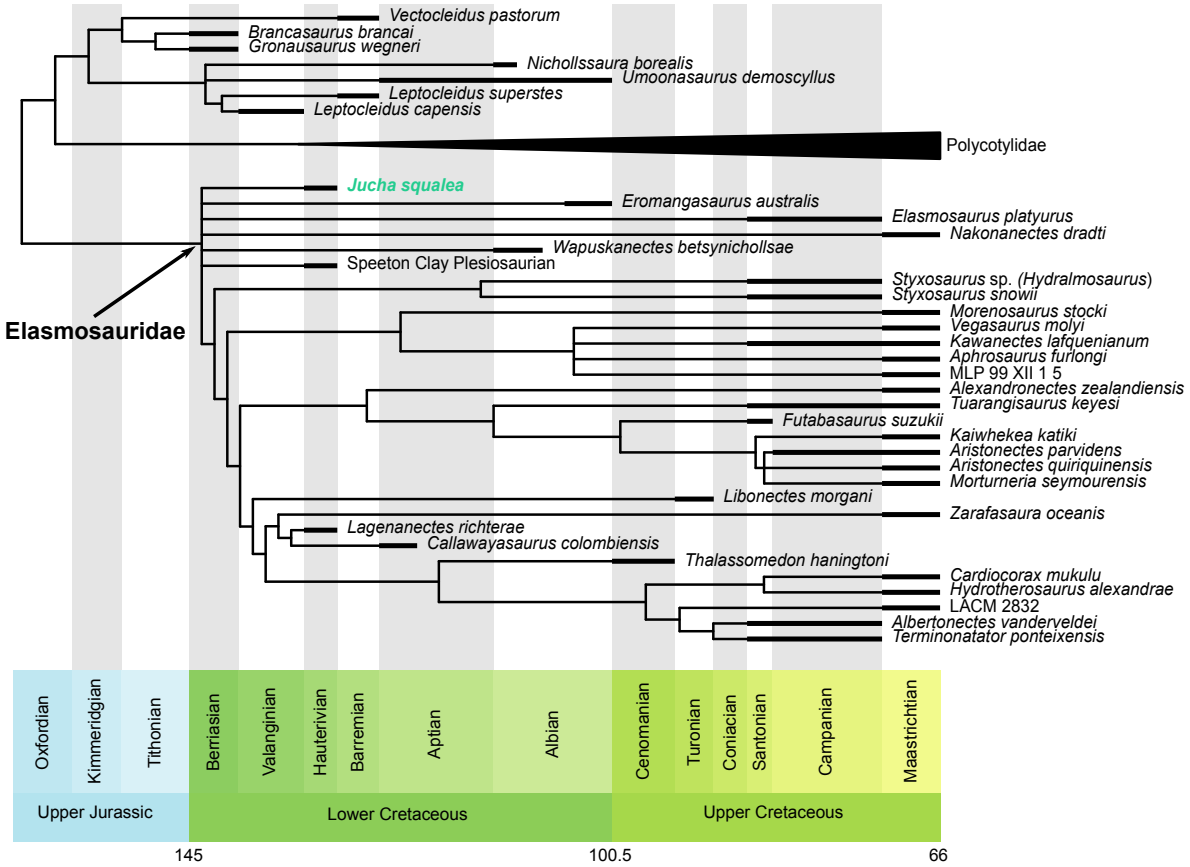

Figure 9. Phylogeny of xenopsarian plesiosaurians: time-scaled strict consensus of the implied weighting maximum parsimony analysis. The analysis was conducted on Plesiosauria as a whole, but only the relevant subset is presented here (see also Supporting Information, Figs S1, S2). Despite a polytomy at the base of Elasmosauridae, *Jucha squalea* is recovered as a basal elasmosaurid.

We recover *J. squalea* as one of the most basal elasmosaurids (Fig. 9), regardless of the optimality criterion used. However, basal polytomies are recovered in both the equal and implied weighting analyses, involving taxa frequently regarded as early elasmosaurids. For the implied weighting, this basal polytomy contains *Er. australis*, *Wa. betsynichollsae* and postcranial skeletons not yet formally described from the Hauterivian of the Speeton Clay Formation of England (NHMUK PV R8623 and SCARB 200751), known as the 'Speeton Clay Plesiosaurian' (Benson & Druckenmiller, 2014; Otero, 2016; Sachs *et al.*, 2017; Serratos *et al.*, 2017; O'Gorman, 2020). Unexpectedly, two elasmosaurine OTUs join this basal polytomy: *El. platyurus* and *N. bradti*. The basal polytomy is much larger in the equal weight analysis, mainly because the Maastrichtian taxon *Alexandronectes parvidens* Cabrera, 1941 (whose scores were not altered from O'Gorman, 2020) is often recovered as a basal xenopsarian. In equal weights, *J. squalea* forms a clade of early elasmosaurids with *Callawayasaurus*

colombiensis and *Er. australis* (Supporting Information, Fig. S2). The clade Elasmosaurinae is recovered as in the study by O'Gorman (2020), in addition to non-aristonectine weddellonectians (Supporting Information, Fig. S2). The support for the trees arising from each method is low, as in the original analysis [although O'Gorman (2020) estimated support via a Bremer decay index, whereas we used symmetric resampling]. No method yields a better supported topology than the other, although the support for Elasmosauridae is slightly better in implied weighting than in equally weights (21 vs. 19; see Supporting Information, Figs S3, S4).

The addition of *J. squalea* and *La. richterae* and the implied weighting framework result in most parsimonious trees that differ substantially from those of O'Gorman (2020). Generally, the topology we recovered in implied weighting appears less congruent with stratigraphy: *La. richterae* and *Callawaysaurus colombiensis* are recovered as fairly derived, closely related to the Late Cretaceous taxa *Albertonectes vanderveldei*, *Cardiocorax mukulu* Araújo et al. 2015, *H. alexandrae*, *Li. morgani*, *Th. haningtoni* and *Z. oceanis*. This has the effect of dragging several deeply nested nodes into the Early Cretaceous. In this topology, the clade Euelasmosaurida is restricted to a single OTU, *Li. morgani*. Weddelonectians are recovered as closely related, but the clade as presently defined is paraphyletic in our consensus tree. The clade with the most profound modifications is Elasmosaurinae, whose members are recovered as either basal (*El. platyurus* and *N. bradti*) or derived forms (*Albertonectes vanderveldei*, *H. alexandrae* and *Terminonatator ponteixensis* Sato, 2003).

Patterns of cervical elongation

Phylogenetic uncertainties set aside, *J. squalea* unambiguously represents an early attempt at cervical elongation (Fig. 10; Supporting Information, Fig. S5), recording high length-to-height ratios compared with other Early Cretaceous taxa. Indeed, the holotype of *J. squalea* (1.36) is surpassed only by *Er. australis*(1.37), cf. *Jucha* (1.4), an indeterminate elasmosaurid from the Valanginian of Russia (1.41) and some cervical centra of the holotype of '*Woolungasaurus glendowerensis*' (1.51; regarded as an indeterminate Aptian elasmosaurid by Kear, 2007), which differs from the much lower values of *Callawayasaurus colombiensis* (1.19), *La. richterae* (1.06) and non-elasmosaurid xenopsarians (0.80–0.92). The lowest value among Early Cretaceous elasmosaurids is that of the anterior cervicals of '*Cimoliasaurus maccoyi*' Etheridge, 1904 (another indeterminate Aptian elasmosaurid Kear, 2002a), with a value of 0.97 (more posterior cervicals record a higher value of 1.19). The full range of cervical elongation values recorded by Early Cretaceous elasmosaurids (0.97–1.51) is thus substantial (Fig.

10; Supporting Information, Fig. S5), but still a far cry from what elasmosaurids evolved during the Late Cretaceous, especially during the Campanian–Maastrichtian interval (0.9–1.8).

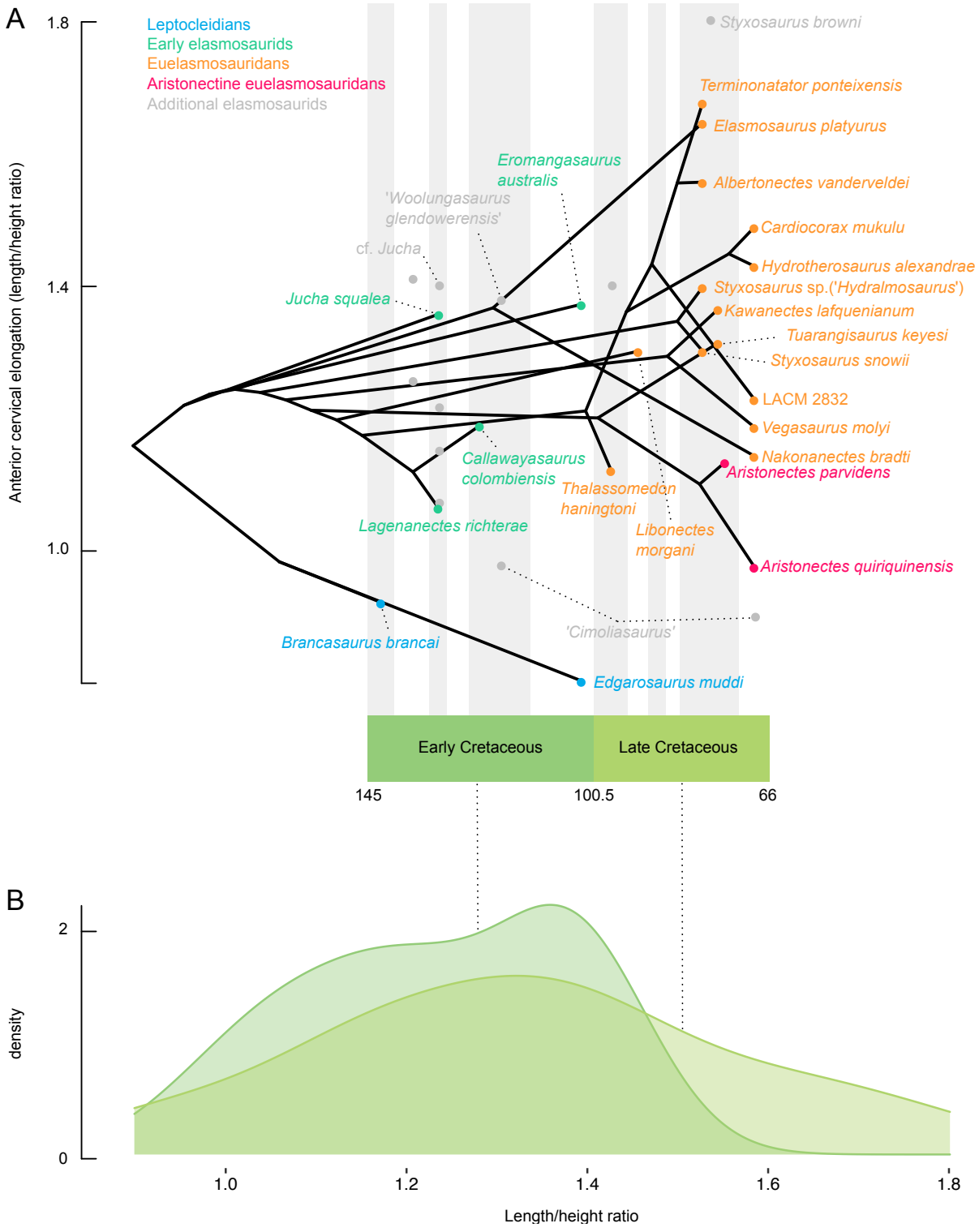

Figure 10. Patterns of vertebral elongation in anterior cervical centra in elasmosaurids. A, phenogram using the anterior cervical centra (at or close to the tenth cervical

centrum); additional elasmosaurids not included in the phylogeny have also been mapped (grey dots). B, density distribution of cervical elongation values for the Early and Late Cretaceous.

Several taxa exceed the value of *J. squalea* during the Late Cretaceous: *Albertonectes vanderveldei*, *Cardiocorax mukulu*, *El. platyurus*, *H. alexandrae*, *Styxosaurus* spp. and *Te. ponteixensis*. Although there is evidence that elamosaurid taxa as a whole record longer cervical centra during the Late Cretaceous (Fig. 10; Supporting Information, Fig. S5), the uncertainties of the phylogenetic relationships of elasmosaurids (see above) and the indeterminate status of 'cimoliasaurids' make it hard to identify unambiguous episodes of cervical reduction, besides *N. bradti* and aristonectines (Serratos *et al.*, 2017).

DISCUSSION

Neck length in sauropterygians is more strongly driven by changes in the number of vertebra than by a modification of their individual shape (Soul & Benson, 2017). As a result, the incomplete preservation of the neck in the type specimen precludes a precise evaluation of the length of the neck of *J. squalea*. However, centrum shape also remains an important parameter, and the data of Soul & Benson (2017) indicate that the number of cervical centra in long-necked plesiosaurians is well correlated (Pearson's $r = 0.8$, $P < 0.001$; see Supporting Information, Table S2) with their average length. Cervical centrum elongation is thus a useful parameter to investigate neck elongation when complete skeletons are missing, as is the case for the early evolution of elasmosaurids. The anterior cervical centra of *J. squalea* are clearly more elongated than those of other early xenopsarians, yielding one of the highest values of the Early Cretaceous; it now appears clear that elasmosaurids attained a substantial range of cervical elongation values early in their history (Fig. 10; Supporting Information, Fig. S5), thanks to the co-occurrence of *J. squalea*, *La. richterae* and indeterminate elasmosaurids from the Valanginian–Hauterivian interval of Russia and Argentina (O'Gorman *et al.*, 2015a; Sachs *et al.*, 2017; Zverkov & Kiselev, 2018). However, this range is dwarfed by that of Campanian–Maastrichtian elasmosaurids (Fig. 10; Supporting Information, Fig. S5), and our results corroborate the hypothesis of a complex rather than trended evolution of relative neck lengths in elasmosaurids (see Serratos *et al.*, 2017).

Jucha squalea departs from many other elasmosaurids, including Early Cretaceous ones, by possessing bulky propodials and by lacking a median pectoral bar and a heart-shaped intercoracoid fenestra. Despite a generally

poor fossil record, Early Cretaceous elasmosaurids appear dissimilar, displaying a range of coracoid and propodial shapes, with varying degrees of elongation and postaxial deflection (Fig. 11). This, in turn, suggests that these taxa did not differ only in relative neck lengths but also in the shapes of their flippers. Although it is tempting to use this as evidence for high early disparity in elasmosaurids [which appears common in xenopsarians, being documented in leptocleidians (Benson *et al.*, 2013) and polycotylids (Fischer *et al.*, 2018)], only an increased sampling among early elasmosaurids could determine how peculiar the morphologies of *Jucha*, *Callawayasaurus*, *Lagenanectes* and *Wapuskanectes* are.

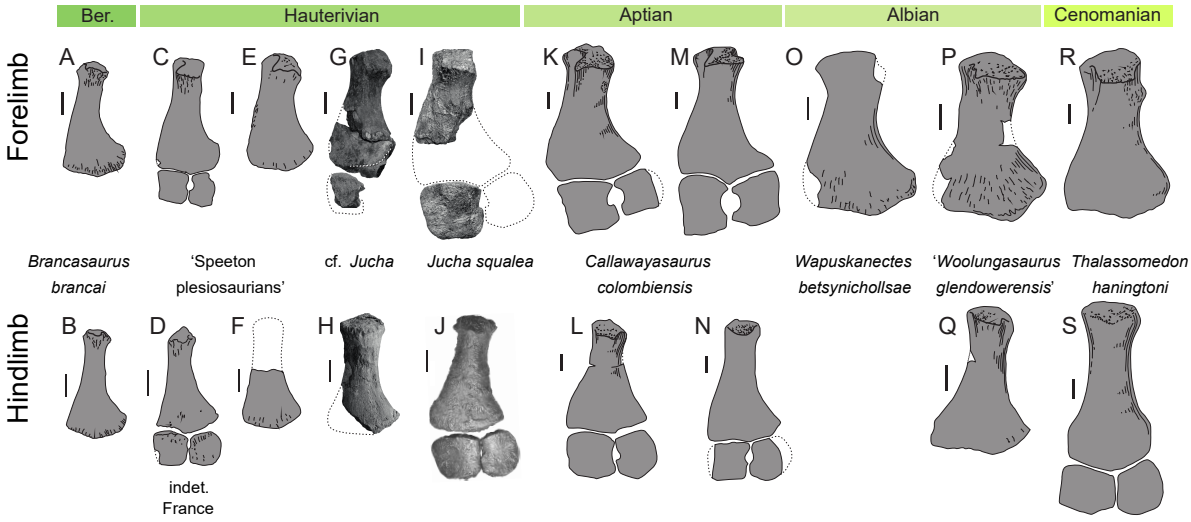

Figure 11. Comparative anatomy of Berriasian–Cenomanian long-necked leptocleidian (A, B) and elasmosaurid (C–S) limbs (propodial + epipodium). A, B, *Brancasaurus brancai* [holotype, GPMM A3.B4; modified from Sachs et al. (2016), mirrored for comparative purposes]. C, E, F, the so-called Speeton Clay plesiosaurians (C, SCARB 200751; E, F, NHMUK PV R8623; based on personal observations by N. G. Zverkov). D, indeterminate elasmosaurid from France (modified from Fournier et al., 1982). G, H, cf. *Jucha* (G, UPM NV 15; H, YKM 65729 + 66119, mirrored for comparative purposes). I, J, *Jucha squalea* (UPM 2756/1-53). K–N, *Callawayasaurus colombiensis* (K, L, holotype UCMP 38349; M, N, referred specimen SGC MGJRG.2018.V.1; both modified from Welles, 1962). O, *Wapuskanectes betsynichollsae* (TMP 98.49.02, in ventral view, modified from Druckenmiller & Russell, 2006). P, Q, indeterminate elasmosaurid [holotype of '*Woolungasaurus glendowerensis*' QM D 6890; QMF3567 in Sachs (2004), modified from Persson (1960) and mirrored for comparative purposes]. R, S, *Thalassomedon haningtoni* (holotype, CMNH 1588, modified from Welles, 1962). All specimens (except for O) are shown in dorsal view. Scale bars: 50 mm.

An unstable phylogenetic signal is another factor currently preventing a thorough understanding of the elasmosaurid diversification. Our analyses of

the dataset from O'Gorman (2020) in implied and equal weighting frameworks yielded topologies that are, in places, clearly at odds with those obtained by the original author, and which were used to define or redefine suprageneric clades. This suggests that at least some of the features that support Elasmosaurinae and Euelasmosaurida might be homoplastic. However, this mismatch is not a new problem; the instability of elasmosaurid relationships has been discussed by Serratos *et al.* (2017), who found low congruence between the results of the analyses of the last semi-decade. At any rate, the wealth of new elasmosaurid data published in the recent years coupled with the ever-increasing knowledge on the behaviour of phylogenetic methods and parameters (Bapst *et al.*, 2016; O'Reilly *et al.*, 2016; Rosa *et al.*, 2019; Smith, 2019) might solve this long-standing conundrum, along with increased and optimized taxonomic and character sampling.

Conclusions

We describe a new basal elasmosaurid from the upper Hauterivian of European Russia, *J. squalea*. This taxon represents one of the geologically oldest occurrences of elasmosaurids. It lacks a series of features that otherwise characterize the group, such as the pectoral bar and the heart-shaped intercoracoid fenestra, and thus documents some of the earliest stages of the elasmosaurid radiation. *Jucha squalea* marks an early attempt at cervical elongation in elasmosaurids via differential growth, possessing anterior cervical centra that are much more elongated than those of other early xenopsaurians. The cervical shape values we gathered suggest that elasmosaurids underwent multiple episodes of cervical shortening, notably during the Early Cretaceous. However, the precise patterns of cervical elongation and character acquisition in elasmosaurids are obscured by an unstable phylogenetic signal. Indeed, our implied weighting maximum parsimony analysis does not recover the clades Euelasmosaurida, Aristonectinae and Elasmosaurinae as currently defined, suggesting that homoplasy plays a pervasive role in elasmosaurid phylogenetics.

SUPPORTING INFORMATION

Additional Supporting Information may be found in the online version of this article at the publisher's web-site:

https://oup.silverchair-cdn.com/oup/backfile/Content_public/Journal/zoolinnean/PAP/10.1093_zoolinnean_zlaa103/1/zlaa103_suppl_supplementary-materials.zip?Expires=1605898260&Signature=GscB6LPn0TDfc1EQGOX

HaiA3zr8TBZ5fN5gqQEaSo9MvZIg~5avrqtXLOubnm-wzpBEJcvs~wmmRwL0z-RxOUPui25AETbkgVndlB0sXsz0cMF5k3ZsFMCKEp-xAfHJxz9rJFEg3p6oVJ~ta12sxGYQvQYLiYbiAI8Qj4vBop5wpydzx6OSesy1P-gbYcovOIk2vV2IlMn1gqFn4TOw7Z1uvr6Nr89iBmP-ldlHQnS78W-tX9u4oOJSr8~l-ZGXx4IH~dmKp58j~jAiQvuVF6IST8xw13UyPwHCtYHhBho5lkAiqeJO20rh2NcaY-~XbLJ7U7j0AetbcSkrXym9XOw__&Key-Pair-Id=APKAIE5G5CRDK6RD3PGA

Table S1. Temporal data used to provide a time scale for the phylogenetic tree. See also the Supporting Information (supplementary file 10 'SUPP_ranges.txt').

Table S2. Body plan from Soul & Benson (2017), focusing on long-necked plesiosaurians (i.e. with Triassic sauropterygians, thalassophoneans, rhomaleaosaurids and polycotylids removed). The contribution column ('contrib') indicates the average length of cervical centra, obtained by dividing the length of the neck by the number of cervical centra. See Soul & Benson (2017) and references therein for the data source. See also the Supporting Information (supplementary file 'SUPP_S&B2017_long_necked.csv').

Figure S1. Strict consensus of the most parsimonious trees arising from our implied weight cladistic analysis.

Figure S2. Strict consensus of the most parsimonious trees arising from our equal weight cladistic analysis.

Figure S3. Clade support by symmetric resampling, implied weighting analysis.

Figure S4. Clade support by symmetric resampling, equal weighting analysis.

Figure S5. Patterns of vertebral elongation in cervical centra in elasmosaurids. A, phenogram using the relatively longest centra of the neck, regardless of its position; additional elasmosaurids not included in the phylogeny have also been mapped (grey dots). B, density distribution of cervical elongation values for the Early and Late Cretaceous.

ACKNOWLEDGEMENTS

We warmly thank the staff at the YKM (Ulyanovsk, Russia) and QM (Hendra, Australia) for their help and care. We thank the Willi Hennig Society for their sponsorship, making TNT available for all researchers free of cost. We warmly thank Sven Sachs and one anonymous reviewer for their help in making this paper better and more intelligible. We thank Dmitry Pashchenko (Paleontological Institute, Moscow, Russia) for help with Latin grammar. The following grants supported the work of V.F.: Newton International Fellowship from the Royal Society (grant NF140022), a Vocatio grant (class of 2014) and a Chargé de Récherches fellowship from the Fonds de la Recherche Scientifique-FNRS (proposal 22319121). The work of N.G.Z. was supported by the state program 0135-2019-0066 (Geological Institute of the Russian Academy of Sciences). We declare we have no competing interests.

REFERENCES

Araújo R, Polcyn MJ, Lindgren J, Jacobs LL, Schulp AS, Mateus O, Gonçalves AO, Morais ML. 2015a. New aristonectine elasmosaurid plesiosaur specimens from the Early Maastrichtian of Angola and comments on paedomorphism in plesiosaurs. Netherlands Journal of Geosciences 94: 93–108.

Araújo R, Polcyn MJ, Schulp AS, Mateus O, Jacobs LL, Olímpio Gonçalves A, Morais M. 2015b. A new elasmosaurid from the early Maastrichtian of Angola and the implications of girdle morphology on swimming style in plesiosaurs. Netherlands Journal of Geosciences 94: 109–120.

Bapst DW. 2012. paleotree: an R package for paleontological and phylogenetic analyses of evolution. Methods in Ecology and Evolution 3: 803–807.

Bapst DW, Wright AM, Matzke NJ, Lloyd GT. 2016. Topology, divergence dates, and macroevolutionary inferences vary between different tip-dating approaches applied to fossil theropods (Dinosauria). Biology Letters 12: 20160237.

Baraboshkin EY. 2004. [Lower Cretaceous ammonite-based zonal standard of the boreal belt] [in Russian]. Bulletin of the Moscow Society of Naturalists. Geological series 79: 44–68.

Baraboshkin EY, Alekseev AS, Kopaevich LF. 2003. Cretaceous palaeogeography of the north-eastern Peri-Tethys. Palaeogeography, Palaeoclimatology, Palaeoecology 196: 177–208.

Baraboshkin EY, Blagoveschensky IV. 2010. [Reference sections of the Upper Jurassic and Lower Cretaceous of the Ulyanovsk] [in Russian]. 5th all-Russian conference 'The Cretaceous system of Russia: problems of stratigraphy and paleogeography' (August 27–28, 2010, Ulyanovsk). Ulyanovsk: Ulyanovsk State University, 1–38.

Baraboshkin EY, Guzhikov AY. 2015. [On suite division of the Hauterivian and Barremian deposits of the Middle Volga Region] [in Russian]. [Bulletin of the regional Interdepartmental Stratigraphical Commission on center and south of the Russian Platform] [in Russian] 6: 83–96.

Baraboshkin EY, Guzhikov AY. 2018. [The Boreal Lower Cretaceous of Russia: revision of the stage boundaries on the base of non-paleontological data] [in Russian]. In: Baraboshkin EY, Lipnitskaya TA, Guzhikov AY, eds. Cretaceous system in Russia and the near abroad: the problems of stratigraphy and palaeogeography. Proceedings of IX All-Russian Meeting. 17–21 September 2018. Belgorod: Polyterra, 47–53.

Bell MA, Lloyd GT. 2015. strap: an R package for plotting phylogenies against stratigraphy and assessing their stratigraphic congruence. Palaeontology 58: 379–389.

Benson RBJ, Druckenmiller PS. 2014. Faunal turnover of marine tetrapods during the Jurassic–Cretaceous transition. Biological Reviews of the Cambridge Philosophical Society 89: 1–23.

Benson RBJ, Ketchum HF, Naish D, Turner LE. 2013. A new leptocleidid (Sauropterygia, Plesiosauria) from the Vectis Formation (early Barremian–early Aptian; Early Cretaceous) of the Isle of Wight and the evolution of Leptocleididae, a controversial clade. Journal of Systematic Palaeontology 11: 231–248.

Berezin AY, Aleksandrov AN. 2016. [Geology and taphonomy of a plesiosaur and a chimaerid fish from the Hauterivian stage of the Cretaceous of Prisursky nature reserve] (in Russian). Natural Science Research in Chuvashia 3: 38–46.

Blagovetshenskiy IV, Shumilkin IA. 2006a. Gastropod mollusks from the Hauterivian of Ulyanovsk (Volga Region): 1. Family aporrhaidae. Paleontological Journal 40: 34–45.

Blagovetshenskiy IV, Shumilkin IA. 2006b. Gastropods of Hauterivian deposits Ulyanovsk Volga region. Genera Khetella Besel, 1977 and Cretadmete gen. nov. Paleontologicheskii Zhurnal 2: 29–33.

Brown D. 1981. The English Upper Jurassic Plesiosauroidea (Reptilia) and a review of the phylogeny and classification of the Plesiosauria. Bulletin of the British Museum (Natural History) Geology 35: 253–347.

Brusatte SL, Benton MJ, Ruta M, Lloyd GT. 2008. Superiority, competition, and opportunism in the evolutionary radiation of dinosaurs. Science (New York, N.Y.) 321: 1485–1488.

Buchy MC. 2005. An elasmosaur (Reptilia: Sauropterygia) from the Turonian (Upper Cretaceous) of Morocco. Carolinea 63: 5–28.

Druckenmiller PS. 2002. Osteology of a new plesiosaur from the Lower Cretaceous (Albian) Thermopolis Shale of Montana. Journal of Vertebrate Paleontology 22: 29–42.

Druckenmiller PS, Russell AP. 2006. A new elasmosaurid plesiosaur (Reptilia: Sauropterygia) from the Lower Cretaceous Clearwater Formation, northeastern Alberta, Canada. Paludicola 5: 184–199.

Dubeikovsky SG, Ochev VG. 1967. [On the remains of plesiosaurs from the Jurassic and Cretaceous deposits of the basin of the upper course of the river Kama] [in Russian]. Voprosy Geologii Yuzhnogo Urala i Povolzh'ya, 4. 97–103 .

Fischer V, Arkhangelsky MS, Stenshin IM, Uspensky GN, Zverkov NG, Benson RB. 2015. Peculiar macrophagous adaptations in a new Cretaceous pliosaurid. Royal Society Open Science 2: 150552.

Fischer V, Benson RBJ, Druckenmiller PS, Ketchum HF, Bardet N. 2018. The evolutionary history of polycotylid plesiosaurians. Royal Society Open Science 5: 172177.

Fischer V, Benson RBJ, Zverkov NG, Soul LC, Arkhangelsky MS, Lambert O, Stenshin IM, Uspensky GN, Druckenmiller PS. 2017. Plasticity and convergence in the evolution of short-necked plesiosaurs. Current Biology: CB 27: 1667–1676.e3.

Fournier R, Jullien R, Lange-Badré B. 1982. Première découverte de restes de Plésiosaure (Reptilia, Sauropsida) au mont Luberon (Vaucluse). Bulletin du Musée d'Histoire Naturelle de Marseille 42: 43–50.

Gasparini Z, Fernandez M, Bardet N, Martin JE, Fernandez M. 2003. The elasmosaurid plesiosaur Aristonectes cabrera from the latest Cretaceous of south America and Antarctica. Journal of Vertebrate Paleontology 23: 104–115.

Gasparini Z, O'Gorman JP. 2014. A new species of Pliosaurus (Sauropterygia, Plesiosauria) from the Upper Jurassic of northwestern Patagonia, Argentina. Ameghiniana 51: 269–283.

Goloboff PA, Catalano SA. 2016. TNT version 1.5, including a full implementation of phylogenetic morphometrics. Cladistics 32: 221–238.

Goloboff PA, Farris JS, Källersjö M, Oxelman B, Ramírez MJ, Szumik CA. 2003. Improvements to resampling measures of group support. Cladistics 19: 324–332.

Hampe O. 1992. Ein grosswüchsiger Pliosauride (Reptilia, Plesiosauria) aus der Unterkreide (oberes Aptium) von Kolumbien. Courier Forschungsintitut Senckenberg 145: 1–32.

Hampe O. 2013. The forgotten remains of a leptocleidid plesiosaur (Sauropterygia: Plesiosauroidea) from the Early Cretaceous of Gronau (Münsterland, Westphalia, Germany). Paläontologische Zeitschrift 87: 473–491.

Hiller N, O'Gorman JP, Otero RA, Mannering AA. 2017. A reappraisal of the Late Cretaceous Weddellian plesiosaur genus Mauisaurus Hector, 1874. New Zealand Journal of Geology and Geophysics 60: 112–128.

Kabanov KA. 1959. [Features of the freshening of the Hauterivian sea in Ulyanovsk Volga region] [in Russian]. Doklady Akademii Nauk SSSR 124: 893–895.

Kear BP. 2002a. Reassessment of the Early Cretaceous plesiosaur Cimoliasaurus maccoyi Etheridge, 1904 (Reptilia: Sauropterygia) from White Cliffs, New South Wales. Australian Journal of Zoology 50: 671–685.

Kear BP. 2002b. Elasmosaurid skull from the Lower Cretaceous of Queensland (Reptilia: Sauropterygia). Australian Journal of Zoology 50: 671–685.

Kear BP. 2005. A new elasmosaurid plesiosaur from the Lower Cretaceous of Queensland, Australia. Journal of Vertebrate Paleontology 25: 792–805.

Kear BP. 2007. Taxonomic clarification of the Australian elasmosaurid genus Eromangasaurus, with reference to other austral elasmosaur taxa. Journal of Vertebrate Paleontology 27: 241–246.

Kear BP, Schroeder NI, Lee MS. 2006. An archaic crested plesiosaur in opal from the Lower Cretaceous high-latitude deposits of Australia. Biology Letters 2: 615–619.

Kubo T, Mitchell MT, Henderson DM. 2012. Albertonectes vanderveldei, a new elasmosaur (Reptilia, Sauropterygia) from the Upper Cretaceous of Alberta. Journal of Vertebrate Paleontology 32: 557–572.

Lazo DG, Cichowolski M. 2003. First Plesiosaur remains from the Lower Cretaceous of the Neuquén Basin, Argentina. Journal of Paleontology 77: 784–789.

Lomax DR, Wahl WR. 2013. A new specimen of the elasmosaurid plesiosaur Zarafasaura oceanis from the Upper Cretaceous (Maastrichtian) of Morocco. Paludicola 9: 97–109.

Madzia D, Cau A. 2020. Estimating the evolutionary rates in mosasauroids and plesiosaurs: discussion of niche occupation in Late Cretaceous seas. PeerJ 8: e8941.

Madzia D, Sachs S, Lindgren J. 2018. Morphological and phylogenetic aspects of the dentition of Megacephalosaurus eulerti, a pliosaurid from the Turonian of Kansas, USA, with remarks on the cranial anatomy of the taxon. Geological Magazine 156: 1201–1216.

Noè LF, Taylor MA, Gómez-Pérez M. 2017. An integrated approach to understanding the role of the long neck in plesiosaurs. Acta Palaeontologica Polonica 62: 137–162.

O'Gorman JP. 2016. A small body sized non-aristonectine elasmosaurid (Sauropterygia, Plesiosauria) from the Late Cretaceous of Patagonia with comments on the relationships of the Patagonian and Antarctic elasmosaurids. Ameghiniana 53: 245–268.

O'Gorman JP. 2020. Elasmosaurid phylogeny and paleobiogeography, with a reappraisal of Aphrosaurus furlongi from the Maastrichtian of the Moreno Formation. Journal of Vertebrate Paleontology 39: e1692025.

O'Gorman JP, Gasparini Z, Spalletti LA. 2018. A new Pliosaurus species (Sauropterygia, Plesiosauria) from the Upper Jurassic of Patagonia: new insights on the Tithonian morphological disparity of mandibular symphyseal morphology. Journal of Paleontology 92: 240–253.

O'Gorman JP, Lazo DG, Luci L, Cataldo CS, Schwarz E, Lescano M, Aguirre-Urreta MB. 2015a. New plesiosaur records from the Lower Cretaceous of the Neuquén Basin, west-central Argentina, with an updated picture of occurrences and facies relationships. Cretaceous Research 56: 372–387.

O'Gorman JP, Salgado L, Olivero EB, Marenssi SA. 2015b. Vegasaurus molyi, gen. et sp. nov. (Plesiosauria, Elasmosauridae), from the Cape Lamb Member (lower Maastrichtian) of the Snow Hill Island Formation, Vega Island, Antarctica, and remarks on Wedellian Elasmosauridae. Journal of Vertebrate Paleontology 35: e931285.

O'Keefe FR. 2001. A cladistic analysis and taxonomic revision of the Plesiosauria (Reptilia: Sauropterygia). Acta Zoological Fennica 213: 1–63.

O'Keefe FR. 2002. The evolution of plesiosaur and pliosaur morphotypes in the Plesiosauria (Reptilia: Sauropterygia). Palaeobiology 28: 101–112.

O'Keefe FR, Chiappe LM. 2011. Viviparity and K-selected life history in a Mesozoic marine plesiosaur (Reptilia, Sauropterygia). Science (New York, N.Y.) 333: 870–873.

O'Keefe FR, Hiller N. 2006. Morphologic and ontogenetic patterns in elasmosaur neck length, with comments on the taxonomic utility of neck length variables. Paludicola 5: 206–229.

O'Keefe FR, Street HP, Wilhelm BC, Richards CD, Zhu H. 2011. A new skeleton of the cryptoclidid plesiosaur Tatenectes laramiensis reveals a novel body shape among plesiosaurs. Journal of Vertebrate Paleontology 31: 330–339.

O'Reilly JE, Puttick MN, Parry L, Tanner AR, Tarver JE, Fleming J, Pisani D, Donoghue PC. 2016. Bayesian methods outperform parsimony but at the expense

of precision in the estimation of phylogeny from discrete morphological data. Biology Letters 12: 20160081.

Otero RA. 2016. Taxonomic reassessment of Hydralmosaurus as Styxosaurus: new insights on the elasmosaurid neck evolution throughout the Cretaceous. PeerJ 4: e1777.

Otero RA, O'Gorman JP, Hiller N, O'Keefe FR, Fordyce RE. 2016. Alexandronectes zealandiensis gen. et sp. nov., a new aristonectine plesiosaur from the lower Maastrichtian of New Zealand. Journal of Vertebrate Paleontology 36: e1054494.

Otero RA, Soto-Acuña S, O'Keefe FR, O'Gorman JP, Stinnesbeck W, Suárez ME, Rubilar-Rogers D, Salazar C, Quinzio-Sinn LA. 2014. Aristonectes quiriquinensis, sp. nov., a new highly derived elasmosaurid from the upper Maastrichtian of central Chile. Journal of Vertebrate Paleontology 34: 100–125.

Owen R. 1840. Report on British fossil reptiles. Report of the British Association for the Advancement of Science 9: 43–126.

Paradis E, Claude J, Strimmer K. 2004. APE: Analyses of Phylogenetics and Evolution in R language. Bioinformatics (Oxford, England) 20: 289–290.

Páramo-Fonseca ME. 2015. Estado actual del conocimiento de los reptiles marinos cretácicos. In: Fernández M, Herrera Y, eds. Reptiles Extintos–volumen en homenaje a Zulma Gasparini. Buenos Aires: Publicación Electrónica de la Asociación Paleontológica Argentina, 40–57.

Páramo-Fonseca ME, Benavides-Cabra CD, Gutiérrez IE. 2018. A new large pliosaurid from the Barremian (Lower Cretaceous) of Sáchica, Boyacá, Colombia. Earth Sciences Research Journal 22: 223–238.

Páramo-Fonseca ME, Benavides-Cabra CD, Gutiérrez IE. 2019a. A new specimen of Stenorhynchosaurus munozi Páramo-Fonseca et al., 2016 (Plesiosauria, Pliosauridae), from the Barremian of Colombia: new morphological features and ontogenetic implications. Journal of Vertebrate Paleontology 39: e1663426.

Páramo-Fonseca ME, Gómez-Pérez M, Noé LF, Etayo-Serna F. 2016. Stenorhynchosaurus munozi, gen. et sp. nov. a new pliosaurid from the Upper Barremian (Lower Cretaceous) of Villa de Leiva, Colombia, South America. Revista de la Academia Colombiana de Ciencias Exactas, Físicas y Naturales 40: 84–103.

Páramo-Fonseca ME, O'Gorman JP, Gasparini Z, Padilla S, Parra-Ruge ML. 2019b. A new late Aptian elasmosaurid from the Paja Formation, Villa de Leiva, Colombia. Cretaceous Research 99: 30–40.

Pavlow AP. 1892. Bélemnites de Speeton et leurs rapports avec les bélemnites des autres pays. In: Pavlow AP, Lamplugh GW, eds. Argiles de Speeton et leurs

équivalents. Bulletin de la Société des Naturalistes de Moscou, nova serie 5: 455–570.

Pavlow AP. 1901. Le Crétacé inférieur de la Russie et sa faune. I. Apercu historique des recherches, suivi d'indications sur la distribution des mers et des terres aux différentes époques. II. Céphalopodes du Néocomien supérieur du type de Simbirsk. Nouveaux Mémoires de la Société des Naturalistes de Moscou 16: 1–87.

Persson PO. 1960. Lower Cretaceous plesiosaurians (Rept.) from Australia. Lunds Universitets Arsskrift. 56: 1–23.

Revell LJ. 2012. phytools: an R package for phylogenetic comparative biology (and other things). Methods in Ecology and Evolution 3: 217–223.

Rosa BB, Melo GAR, Barbeitos MS. 2019. Homoplasy-based partitioning outperforms alternatives in Bayesian analysis of discrete morphological data. Systematic Biology 68: 657–671.

Sachs S. 2004. Redescription of Woolungasaurus glendowerensis (Plesiosauria: Elasmosauridae) from the lower cretaceous of northeast Queensland. Memoirs of the Queensland Museum 49: 713–731.

Sachs S. 2005a. Tuarangisaurus australis sp. nov. (Plesiosauria: Elasmosauridae) from the Lower Cretaceous of northeastern Queensland, with additional notes on the phylogeny of the Elasmosauridae. Memoirs of the Queensland Museum 50: 425–440.

Sachs S. 2005b. Redescription of Elasmosaurus platyurus Cope 1868 (Plesiosauria: Elasmosauridae) from the Upper Cretaceous (Lower Campanian) of Kansas, U.S.A. Paludicola 5: 92–106.

Sachs S, Hornung JJ, Kear BP. 2016. Reappraisal of Europe's most complete Early Cretaceous plesiosaurian: Brancasaurus brancai Wegner, 1914 from the "Wealden facies" of Germany. PeerJ 4: e2813.

Sachs S, Hornung JJ, Kear BP. 2017. A new basal elasmosaurid (Sauropterygia: Plesiosauria) from the Lower Cretaceous of Germany. Journal of Vertebrate Paleontology 37: e1301945.

Sachs S, Kear BP. 2015. Postcranium of the paradigm elasmosaurid plesiosaurian Libonectes morgani (Welles, 1949). Geological Magazine 252: 694–710.

Sachs S, Kear BP. 2017. Redescription of the elasmosaurid plesiosaurian Libonectes atlasense from the Upper Cretaceous of Morocco. Cretaceous Research 74: 205–222.

Sachs S, Kear BP, Everhart MJ. 2013. Revised vertebral count in the "longest-necked vertebrate" Elasmosaurus platyurus Cope 1868, and clarification of the cervical-dorsal transition in Plesiosauria. PLoS One 8: e70877.

Sachs S, Lindgren J, Kear BP. 2018. Reassessment of the Styxosaurus snowii (Williston, 1890) holotype specimen and its implications for elasmosaurid plesiosaurian interrelationships. Alcheringa 42: 560–574.

Sato T. 2003. Terminonatator ponteixensis, a new elasmosaur (Reptilia; Sauropterygia) from the Upper Cretaceous of Saskatchewan. Journal of Vertebrate Paleontology 23: 89–103.

Sato T, Hasegawa Y, Manabe M. 2006. A new elasmosaurid plesiosaur from the Upper Cretaceous of Fukushima, Japan. Palaeontology 49: 467–484.

Seeley HG. 1874. Note on some of the generic modifications of the plesiosaurian pectoral arch. Quarterly Journal of the Geological Society 30: 436–449.

Serratos DJ, Druckenmiller P, Benson RBJ. 2017. A new elasmosaurid (Sauropterygia, Plesiosauria) from the Bearpaw Shale (Late Cretaceous, Maastrichtian) of Montana demonstrates multiple evolutionary reductions of neck length within Elasmosauridae. Journal of Vertebrate Paleontology 37: e1278608.

Smith MR. 2019. Bayesian and parsimony approaches reconstruct informative trees from simulated morphological datasets. Biology Letters 15: 20180632.

Soul LC, Benson RBJ. 2017. Developmental mechanisms of macroevolutionary change in the tetrapod axis: a case study of Sauropterygia. Evolution; international journal of organic evolution 71: 1164–1177.

Utsunomiya S. 2019. [Oldest Elasmosauridae (Plesiosauria) in East Asia from the Upper Cretaceous Goshoura Group, Shishijima Island, southwestern Japan] [in Japanese]. Bulletin of the Osaka Museum of Natural History 73: 23–35.

Welles SP. 1943. Elasmosaurid plesiosaurs with description of new material from California and Colorado. Memoirs of the University of California 13: 125–254.

Welles SP. 1949. A new Elasmosaur from the Eagle Ford Shale of Texas. Part I systematic description. Fondren Sciences Series, Southern Methodist University 1: 1–31.

Welles SP. 1952. A review of the North American Cretaceous elasmosaurs. University of California Publications in Geological Sciences 29: 47–144.

Welles SP. 1962. A new species of elasmosaur from the Aptian of Colombia, and a review of the Cretaceous plesiosaurs. University of California Publications in Geological Sciences 44: 1–96.

Welles SP, Bump JD. 1949. Alzadasaurus pembertoni, a new elasmosaur from the Upper Cretaceous of South Dakota. Journal of Paleontology 23: 521–535.

Wiffen J, Moisley WL. 1986. Late Cretaceous reptiles (families Elasmosauridae and Pliosauridae) from the Mangahouanga Stream, North Island, New Zealand. New Zealand Journal of Geology and Geophysics 29: 205–252.

Wintrich T, Scaal M, Sander PM. 2017. Foramina in plesiosaur cervical centra indicate a specialized vascular system. Fossil Record 20: 279–290.

Zverkov NG, Kiselev DN. 2018. Plesiosaurs from the Lower Cretaceous of Glebovo Section, Yaroslavl Region. In: Baraboshkin EY, Lipnitskaya TA, Guzhikov AY, eds. Proceedings of IX All-Russian Meeting Cretaceous system of Russia and near abroad: problems of stratigraphy and paleogeography. 17–21 September 2018. Belgorod: Polyterra, 137–141.